工學博士學位論文

Synthesis, Characterization, and Applications of Comb-Like Polymers having Fluorinated Alkyl Side Group and Stimuli-Responsive Polymers having Cinnamoyl or Oligo(Ethylene Glycol) Side Groups

플루오로 알킬기를 측쇄로 가지는 빗살형 고분자와 시나모일기 또는 올리고(에틸렌 글라이콜)기를 측쇄로 가지는 자극응답성 고분자의 합성, 분석 및 응용

2012年 8月

서울大學校 大學院

化學生物工學部

鄭　在　勝

Synthesis, Characterization, and Applications of Comb-Like Polymers having Fluorinated Alkyl Side Group and Stimuli-Responsive Polymers having Cinnamoyl or Oligo(Ethylene Glycol) Side Groups

by

Jae-Seung Chung

Advisor: Professor Jong-Chan Lee, Ph. D.

Submitted in Partial Fulfillment
of the Requirements for the Degree of
DOCTOR OF PHILOSOPHY

August, 2012

School of Chemical and Biological Engineering
College of Engineering
Graduate School
Seoul National University

Abstract

This study presents the synthesis, characterization, and applications of comb-like fluorinated polymers and stimuli-responsive polymers. Through control over the polymer side chain structures, I investigate the various polymer properties and attempt to apply the polymers to the many applications such as antifouling, antibacterial, healing, and water purification. Comb-like fluoropolymers have many applications in areas such as microelectronics, anti-adhesive coatings, and medical materials on account of their low surface energy values. Because of this, there was much effort to synthesize polymers with fluorinated alkyl segments in the side chains. On the other hand, stimuli-reponsive polymers can adapt to surrounding environments, change the molecular formation, regulate transport of ions and molecules, change wettability and adhesion of different species on external stimuli or convert chemical and biochemical signals into optical, electrical, thermal and mechanical signals, and vice versa. These materials are playing an incresasingly important part in a diverse range of applications, such as drug delivery, diagnostics, tissue engineering, healable materials and smart optical systems.

Firstly, a series of comb-like fluorinated poly(oxyethylene)s having different content of fluoroalkyl side group were prepared to examine the effect of the surface structure variation on the surface properties. When the thin films of the polymers having ≥58 mol % of fluoroalkyl side groups were annealed, surface energy decreases and surface stability against polar liquids improved. This surface property behavior was found to be

correlated with changes of the paracrystalline structure orientation and scattering unit numbers after the annealing process very well. However the average tilt angle and *d*-spacing of the fluoroalkyl side group and the paracrystalline ordering of the thin films did not changes, if any, after the annealing process. Near edge X-ray absorption fine structure (NEXAFS) spectroscopy and grazing incidence X-ray diffraction (GIXD) were used to determine the surface structure and contact angle measurement were conducted to measure the surface properties.

Secondly, silver-perfluorodecanethiolate complexes having superhydrophobic, antifouling, antibacterial properties were prepared by a reaction of silver nitrate with perfluorodecanethiol. When the silver nitrate to perfluorodecanethiol molar ratio was 1/2, silver-perfluorodecanethiolate complexes having hierarchical micro-/nano-sized wire shapes were obtained, and they showed superhydrophobic and antifouling properties. After UV irradiation, silver nanoparticles were generated on the wires, and exhibited antibacterial properties.

Thirdly, a series of polymethacrylate films having different glass transition temperatures (T_g) was synthesized and demonstrated to form healable films with different surface hardnesses. A photo-responsive cinnamoyl side group was used both as a crosslinker to control the surface hardness and as a plasticizer to vary the T_g. Two contrasting factors, chain mobility for healing and surface hardness for mechanical properties, were evaluated with heating and UV irradiation to establish the suitable polymer films and healing condition. We achieved the overall healing process with the

polymethacrylate film containing a photocrosslinkable cinnamoyl side group. This study presents the practical basis for healable polymer approaches and provides the considerable candidates.

Finally, we report on a novel thermo-responsive copolymer with ionic group which could be used as a draw solute for forward osmosis (FO) process. 2-(2'-Methoxyethoxy)ethyl methacrylate (MEO_2MA), characterized by a thermo-responsive group with LCST behavior for the recycling process, was copolymerized with 2-(methacryloyloxy)ethyl trimethylammonium chloride (MTAC), which have ionic group in a capable of demonstrating the high osmotic pressure. By controlling the composition of two monomer, both high osmotic pressure and proper LCST point could be obtained. The copolymers prepared with suitable composition of MEO_2MA:MTAC have the considerable potential for use as a novel draw solute for FO process.

Keywords: Comb-like fluorinated polymer, silver-perfluorodecanethiolate complex, antifouling, stimuli-responsive polymer.

Student Number: 2009-30250

TABLE OF CONTENTS

List of Schemes & Figures

List of Tables

Chapter 1

Introduction

1.1. Motivation

Synthesis of fluorinated polymers and stimuli-responsive polymers for various applications such as surface coating, liquid crystal display, photoresist, antifouling, self-healing, drug delivery, diagnostics, and water purification have attracted much attention because of their unique properties.[1-10] For most polymers it is the side chains that determine properties such as solubility, crystallinity, surface chemistry, and so on. Therefore, the control of the polymer side chain has been relevant to the key issue in many industrial applications and a fundamental science.

Fluorinated polymers have many unique characteristics, among which the oleophobic-hydrophobic nature of fluorinated polymer surfaces and their remarkable chemical resistance stand out. These properties arise due to the low intermolecular forces present in highly fluorinated organic compounds. Furthermore, there are much effort to synthesize polymers with fluorinated alkyl segments in the side chains. [11-13] Up to recently, poly(fluoroalkyl methacrylate)s, poly(p-perfluoalkyl ethylene oxy methyl styrene)s and poly(methyl propenoxy perfluoroalkyl siloxane)s were synthesized and exhibited very low surface energies of 7-12 mN/m. In general, surface energies of these polymers has been described in terms of phase separation in nano-scale between fluorinated (fluorophilic) side chain and hydrogenated (fluorophobic) backbone.[14,15] Additionally, those of hydrophobic surfaces known to show good fouling release properties, whereas the hydrophilic surfaces of polymers with low values of polymer-water interfacial energy,

show resistance to protein adsorption and cell adhesion. The interfacial energy between a surface and water is expected to play an important role in conferring antifouling characteristics to a surface. Non-polar hydrophobic surfaces exhibit high interfacial energy with water. [16-18]

Responsive polymers can be used for a variety of applications, such as switching surfaces and adhesives, protective coatings that adapt to the environment, artificial muscles, sensors and drug delivery. [19-21] Responsive systems can be introduced into many products at a relatively low cost, because oftenonly a very thin coating is required. Providing added functionality with such a coating can enhance the value of a product significantly. Many efforts to obtain the suitable polymer properties for special applications have been established.

Our research group has synthesized polymer brushes that have various kinds of side chains such as hydrophobic fluorinated groups, amphiphilicity hydrophilic-hydrophobic groups and special fuctional groups. [22-28] Expecially, we confirmed that surface properties of fluorinated polymers such as wettability and molecular structures using NEXAFS, XPS, GIXD, and contact angle goniometer. It was found that fluorinated side chains of polymers are well aligned at the surface due to the strong amphiphilicity and fluoroalkyl ordering, and some of these polymers have very low surface energies. And also their antifouling and antibacterial properties were characterized. Additionally, our group has tried to synthesize the versatile polymer materials for various applications such as liquid crytstalline, display, photoresist, fuel cell membrane, healable material, polymer

electrolyte and water purification process. In the next section of this chapter, prior to moving on the experimental results and discussion, brief introduction of fluorinated polymers having low surface energy, healable materials, and polymer draw solute for forward osmosis system will be presented.

1.2. Fluorinated polymers having low surface energy

Fluorinated polymers have a prominent position when low values of surface energy are required. The low surface energy is a key property of these polymers and may prevent attachment and adhesion, and addack or solvation by aqueous solution and most organic solvents. [29,30] Despite the polar nature of the C-F bond because of the high elecronegativity of fluorine compared to carbon, perfluorinated linear alkanes and polymers such as poly(tetrafluoroethylene) (PTFE) ideally have no permanent dipolem moment due to the symmetric distribution of charge in these molecules. The nonpolar nature of fluorinated polymers confers a range of properties, including water repellence, solubility in supercritical carbon dioxide, and low dielectric constant. Fluorinated polymers, by virtue of their low dielectric constant, good dimensional stability, good high temperature stability, and low moisture absorption and low outgassing are being considered as interlayer dielectric materials to separate different circuit layers in microelectronics devices. [31] Although, PTFE may be regarded as the benchmark low surface energy material, this polymer has limitations due to its low oil repellency and to

its microcrystalline surface structure. Considerable research efforts, therefore, are directed towards the development of alternative, non-wettable, low surface energy polymeric materials with good film-forming characteristics.

The strength of the C-F bond increases with the extent of adjacent carbon fluorination, meaning that the longer the fluoroalkyl group, the higher its stability, and hydrophobicity. Therefore, films and coatings from fluorinated polymers have been investigated for a variety of applications ranging from low friction aliognment layers in electro-optic devices to surface-modified membranes and to biologically inert coronary stent coatings. (Figure 1.1.)

1.3. Healable materials

In view of the extensive use of polymers and polymer-composites in modern technologies, much recent research has focused on the creation of organic materials that are able to heal and repair themselves, either autonomically or inresponse to some form of stimulus such as heat or light. Healable polymeric materials fall into two broad classes, differentiated by whether an external stimulus is needed to promote the healing process. Autonomically healable materials, once fractured, regain the physical properties of the pristine material without such external intervention, irreversible system. In contrast, reversible system materials regain their original physical properties in response to a specific external stimulus. [32-35]

Irreversible systems are polymeric systems that cannot be reverted back to their monomeric oligomeric, or non crosslinked state. For such polymers, healing is achieved by a different approach- the use of healing agents, either embedded in the polymer matrix in a dormant form such as microcapsule or vascular system. [36-38, Figure 1.2]

Reversible systems are broadly defined as polymeric systems that can revert to either their monomeric, oligomeric, or noncross=linked state. For the polymer to be stable under normal working conditions, the reverting process would normally require an external stimulus for it to occur. For healing purposes, ideally the material would revert to its constituents after cracking but could be reparired by applying the conditions that were used to polymerize it. These systems can be categorized by the nature of the reversible bonds, covalent and noncovalent. [39-40]

1.4. Polymer draw solute for forward osmosis system

Osmosis is the transport of water across a selectively permeable membrane from a region of higher water chemical potential to a region of lower water chemical potential. It is driven by a difference in solute concentrations across the membrane that allows passage of water, but rejects most solute molecules or ions. Forward osmosis (FO) system uses the osmotic pressure differential across the membrane, rather than hydraulic pressure differential (as in reverse osmosis (RO) system), as the driving force for transport of water. The FO process results in concentration of a feed stream and dilution of a highly

concntrated stream referred to as the draw solution. [41-43, Figure 1.3.]

The draw solution on the permeate side of the membrane is the source of the driving force in the FO process. When selecting a draw silution, the main criterion is that it has a higher osmotic pressure than the feed solution. Various chemicals have been suggested and tested as solutes for draw solutions, particularly in seawater desalination applications. [44-47] Another important criterion of FO is the selection of a suitable process for reconcentrating the draw solution after it has been diluted in the FO process. Very often a NaCl solution is used because it has high solubility and is relatively simple to reconcentrate to high concentration with RO without risk of scaling. Diffusion of the solute from the draw solution through the membrane must also be considered. In specific applications where high rehection is desired, multivalent ion solutions may be preferable.

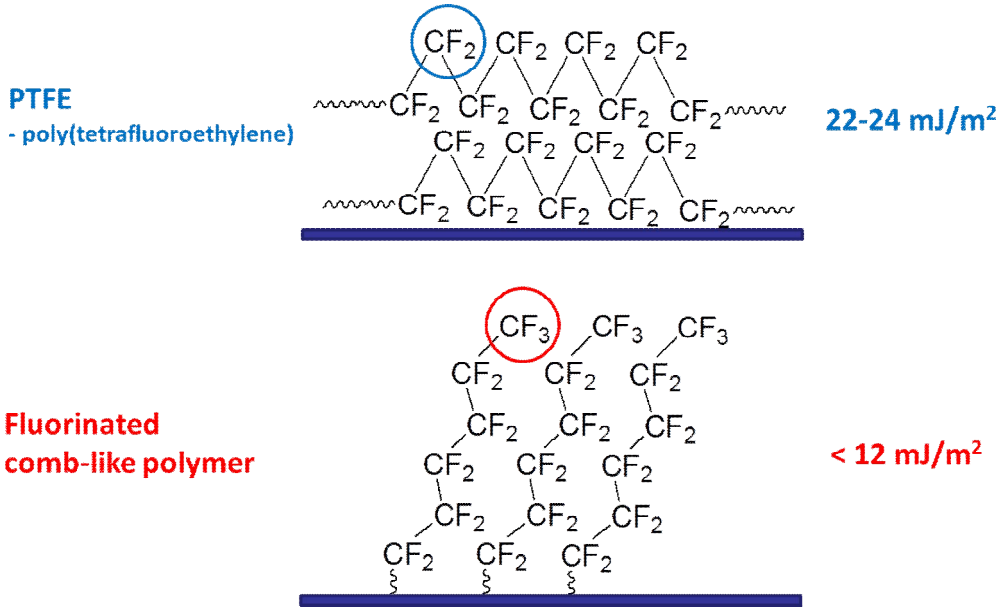

Figure 1.1. Surface energy values of PTFE and fluorinated comb-like polymer.

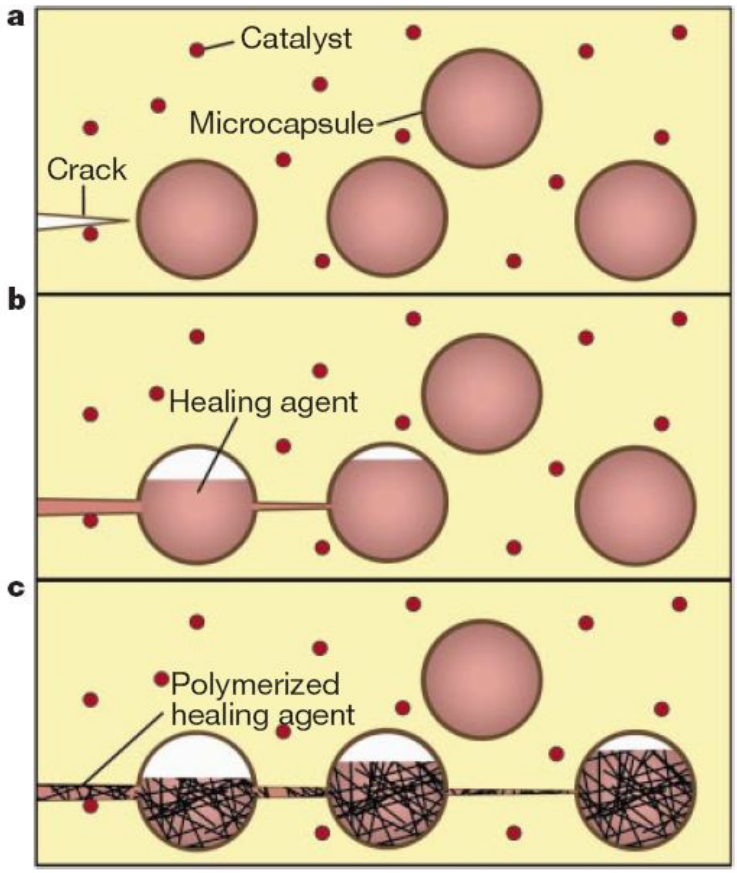

Figure 1.2. The autonomic healing concept. A microencapsulated healing agent is embedded in a structural composite matrix containing a catalyst capable of polymerizing the healing agent. Fig. reproduced from Ref. [36]

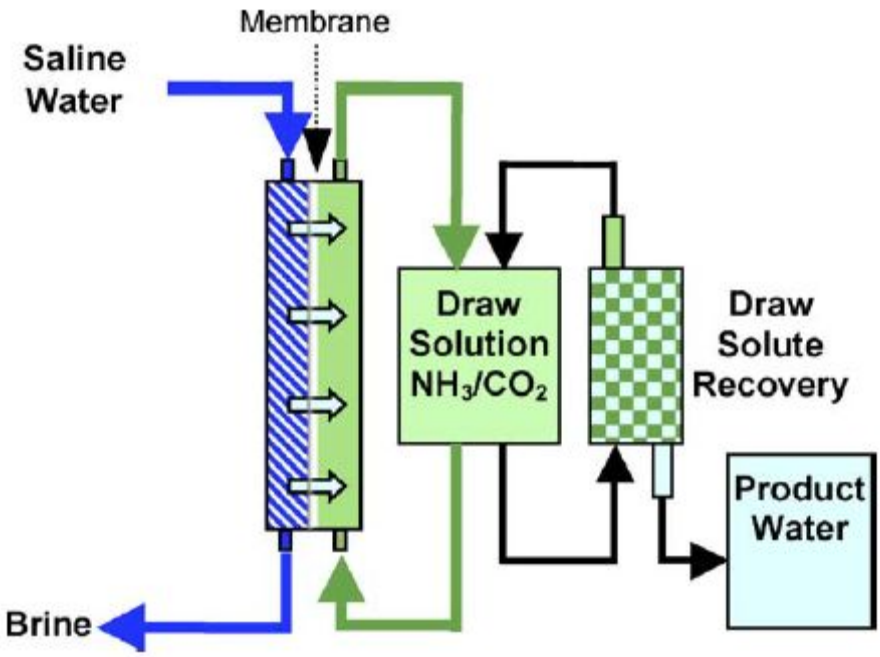

Figure 1.3. Schematic drawing of the ammonia–carbon dioxide FO process. Fig. reproduced from Ref. [43].

1.5. References

[1] Schmidt, D. L.; Coburn, C. E.; Dekoven, B. M.; Potter, G. E.; Meyers, G. F.; Fisher, D. A. *Nature* **1994**, 368, 39.

[2] DeSimone, J. M.; Maury, E. E.; Menceloglu, Y. Z.; McClain, J. B.; Romack, T. J.; Combes, J. R. *Science* **1994**, 265, 356.

[3] Bryan-Brown, G. P.; Wood, E. L.; Sage, I. C. *Nature* **1999**, 399, 338.

[4] Ober, C. K.; Gabor, A. H.; Gallagher-Wetmore, P.; Allen, R. D. *Adv. Mater.* **1997**, 9,1039.

[5] Tsibouklis, J.; Graham, P.; Eaton, P. J.; Smith, J. R.; Nevell, T. G.; Smart, J. D.; Ewen, R. J. *Macromolecules* **2000**, 33, 8460.

[6] Tsibouklis, J.; Thomas, G. N. *Adv. Mater.* **2003**, 15, 647.

[7] Stuart, M. A. C.; Huck, W. T. S.; Genzer, H. Muller, M.; Ober, C. K.; Stamm, M.; Sukhorukov, G. B.; Szleifer, I.; Tsukruk, V. V.; Urban, M.; Winnik, F.; Zauscher, S.; Luzinov, I.; Minko, S. *Nat. Mater.* **2010**, *9*, 101.

[8] Bayer, C. L.; Peppas, N. A. *J. Control. Release* **2008**, *132*, 216

[9] Mendes, P. M. *Chem. Soc. Rev.* **2008**, *37*, 2512.

[10] Luzinov, I.; Minko, S.; Tsukruk, V. V. *Soft Matter.* **2008**, *4*, 714.

[11] Chapman, T.M.; Benrashid, R.; Marra, K. G.; Keener, J. P. *Macromolecules* **1995**, *28*, 331.

[12] Höpken, J.; Möller, M. *Macromolecules* **1992**, *25*, 1461.

[13] Tsibouklis, J.; Stone, M.; Thorpe, A. A.; Graham, P.; Nevell, T. G.; Ewen, R. J. *Langmuir* **1999**, *15*, 7076.

[14] Höpken, J.; Pugh, C.; Richtering, W.; Möller, M. *Makromol. Chem.* **1988**, *189*, 911.

[15] Russell, T. P.; Rabolt, J. F.; Twieg, R. J.; Siemens, R. L.; Farmer, B. L. *Macromolecules* **1986**, *19*, 1135.

[16] Vogler, E. A. in Water in Biomaterials Surface Science, ed. Morra, M., John Wiley & Sons, New York, 2001.

[17] Genzer, J.; Efimenko, K. *Biofouling* **2006**, *22*, 339.

[18] Krishnan, S.; Weinman, C. J.; Ober, C. K. *J. Mater. Chem.* **2008**, *18*, 3405.

[19] Crowe-Willoughby, J. A.; Genzer, J. *J. Am. Chem. Soc.* **2005**, *127*, 17610.

[20] Li, M. H.; Keller, P. *Soft Matter* **2009**, *5*, 927.

[21] Edwards, E. W.; Chanana, M.; Wang, D.; Mohwald, H. *Angew. Chem. Int. Ed.* **2008**, *47*, 320.

[22] Lee, J.-C.; Litt, M. H.; Rogers, C. E. *Macromolecules* **1997**, *30*, 3766.

[23] Lee, J.-C.; Litt, M. H.; Rogers, C. E. *Macromolecules* **1998**, *31*, 2440.

[24] Lee, J.-C.; Oh, K.; Lee, H. B.; Kim, Y. G.; Jho, J. Y.; Kwak, S.-Y.; Park, S.-Y.; Farmer, B. L. *Macromol. Rapid commun.* **2001**, *22*, 815.

[25] Kim, B. G.; Sohn, E.-H.; Cho, K.; Lee, J.-C. *Eur. Polym. J.* **2008**, *44*, 2912.

[26] Kim, B. G.; Chung, J.-S.; Sohn, E.-H.; Kwak, S.-Y.; Lee, J.-C. *Macromolecules* **2009,** *42*, 3333.

[27] Chung, J.-S.; Kim, B. G.; Sohn, E.-H.; Lee, J.-C. *Macromolecules* **2010**, *43*, 10481.

[28] Sohn, E.-H.; Kim, S. H.; Lee, M.; Lee, J.-C.; Song, K. *J. Colloid Interface Sci.* **2011**, *360*, 623.

[29] Krishnan, S.; Kwark, Y.-J.; Ober, C. K. *The Chemical Record* **2004**, *4*, 315.

[30] Martinelli, E.; Menghetti, S.; Galli, G.; Glisenti, A.; Krishnan, S.; Paik, M. Y.; Ober, C. K.; Smilgies, D.-M.; Fischer, D. A. *J. Polym. Sci. Part A: Polym. Chem.* **2009**, *47*, 267.

[31] Wu, S. H. *Polymer Interfaces and Adhesion*, marcel dekker, New York 1982.

[32] Wu, D. Y.; Meure, S.; Solomon, D. *Prog. Polym. Sci.* **2008**, *33*, 479.

[33] Murphy, E. B.; Wudl, F. *Prog. Polym. Sci.* **2010**, *35*, 223

[34] Burattini, S.; Greenland, B. W.; Chappell, D.; Colquhoun, H. M.; Hayes, W. *Chem. Soc. Rev.* **2010**, *39*, 1973.

[35] Hager, M. D.; Greil, P.; Leyens, C.; Van Der Zwaag, S.; Schubert, U. S. *Adv. Mater.* **2010**, *22*, 5424.

[36] White, S. R.; Sottos, N. R.; Geubelle, P. H.; Moore, J. S.; Kessler, M. R.; Sriram, S. R.; Brown, E. N.; Viswanathan, S. *Nature* **2001**, *409*, 794.

[37] Cho, S. H.; Andersson, H. M.; White, S. R.; Sottos, N. R.; Braun, P. V. *Adv. Mater.*

2006, *18*, 997.

[38] Toohey, K. S.; Sottos, N. R.; Lewis, J. A.; Moor, J. S.; White, S. R. *Nat. Mater.* **2007**, *6*, 581.

[39] Ghosh, B.; Urban, M. W. *Science* **2009**, *323*, 1458.

[40] Chung, C.-M.; Roh, Y.-S.; Cho, S.-Y.; Kim, J.-G. *Chem. Mater.* **2004**, *16*, 3982.

[41] Cath, T. Y.; Childress, A. E.; Elimelech, M. *J. Membr. Sci.* **2006**, *281*, 70.

[42] Su, J. C.; Yang, Q.; Teo, J. F.; Chung, T.-S. *J. Membr. Sci.* **2007**, *300*, 6.

[43] McCutcheon, J. R.; McGinnis, R. L.; Elimelech, M. *Desalination*, **2005**, *174*, 1.

[44] Kessler, J. O.; Moody, C. D. *Desalination*, **1975**, *18*, 297.

[45] Kravath, R. E.; Davis, J. A. *Desalination*, **1975**, *16*, 151.

[46] Li, D.; Wang, H. T. *J. Mater. Chem.* **2010**, *20*, 4551.

[47] McCutcheon, J. R.; McGinnis, R. L.; Elimelech, M. *J. Membr. Sci.* **2006**, *278*, 114.

Chapter 2

Molecular Structure and Surface Properties of Comb-Like Fluorinated Poly(oxyethylene)s Having Different Content of Fluoroalkyl Side Group

2.1. Introduction

Fluorinated polymers have been studied intensively because of their excellent properties, such as low surface energy, good chemical and thermal stability, anti-adhesive ability, low friction coefficient, biocompatibility, and non-stick behavior.[1-3] Researchers have particularly focused on comb-like fluorinated polymers for their excellent surface properties arising from the well ordered surface molecular structure for use as water/oil repellent and anti-fouling coating materials.[4-6] In general, the molecular structure of comb-like fluorinated polymer has a key influence on the surface properties, such as the surface energy, stability, adhesion force, repellency and wetting behavior.[7-12] Takahara et al. reported the molecular aggregation structure and surface properties of the poly(fluoroalkyl acrylate)s and poly(fluoroalkyl methacrylate)s having fluoroalkyl side groups with different fluorocarbon lengths and the fluorinated polyacrylates having long fluoroalkyl side groups (number of fluorocarbon $\geq$ 8) were found to have an ordered structure with high water repellency.[13-15] Ober et al. synthesized various fluorinated block copolymers having low surface energy16 and examined their molecular structure using near edge X-ray absorption fine structure (NEXAFS)[17-20] and grazing incidence X-ray diffraction (GIXD) measurement.[21] A previous study examined the effects of side chain interconnecting groups of comb-like fluorinated polystyrenes on the bulk and surface properties.[22] Various reports have been published on the comb-like fluorinated polymers, whereas only a few studies have

investigated the influence of the content of fluoroalkyl side group on the surface properties of comb-like fluorinated polymers.[23-25]

A paracrystal, which is an intermediate stage between a “perfect crystal” and “amorphous structure”, as a “building block”, has become accepted as a basic physical concept for defining certain ordered structures. In molecular structure studies of semicrystalline polymers, several models, including the Hosemann paracrystal model, Cialle model and modified Cialle model have been used to describe ordered polymer structures.[26-28] Recently, the paracrystalline theory proposed by Hosemann[29,30] was considered to be the most suitable model for examining polymer structures having lamellar structures.[13,14,31,32] Indeed, lamellar structures are one of the most common morphological structures observed in polymers, including those in comb-like fluorinated polymers.[13,16,22,31]

Previously, it was reported that comb-like poly(oxyethylene)s containing hydrocarbon alkyl or fluoroalkyl side groups show well ordered structures due to phase separation between the flexible hydrophilic oxyethylene backbone part and hydrophobic side group part.[24,33-40] Furthermore, comb-like poly(oxyethylene)s containing fluoroalkyl side group have very low surface energies owing to the well ordered structures near the outmost surface.[24] This study examined the correlation between the surface properties and molecular structures of comb-like fluorinated poly(oxyethylene)s possessing different contents of fluoroalkyl side group. The Hosemann paracrystal model was used to evaluate the paracrystalline structure ordering and orientation in the polymer thin films. The effect

of the paracrystalline structure ordering and orientation to the surface properties of comb-like fluorinated polymers having different content of fluoroalkyl side group were systematically studied. NEXAFS and GIXD techniques were used to characterize the molecular structures on the surface, and contact angle measurements were performed to analyze the surface properties, such as surface energy and stability.

2.2. Experimental

Materials.

Epichlorohydrin (Aldrich) was dried over calcium chloride and distilled fractionally from calcium oxide. Methylene chloride and methanol were refluxed over calcium hydride and 1,1,2-trichlorotrifluoroethane (F113) was refluxed over calcium chloride and freshly distilled under a nitrogen atmosphere prior to use. *1H,1H,2H,2H*-Perfluorodecanethiol (Aldrich), triphenylcarbenium hexafluorophosphate (Aldrich), sodium (Aldrich), d-chloroform (ACROS) and an ionic liquid, 1-butyl-3-methyl-imidazolium chloride ([bmim][Cl]) (C-TRI), were used without further purification.

Synthesis.

Preparation of poly[oxy(chloromethyl)ethylene]

Triphenylcarbenium hexafluorophosphate (0.05 g, 0.13 mmol) was added to a stirred solution of epichlorohydrin (5.0 g, 54.04 mmol) in 3.78 mL of methylene chloride under a nitrogen atmosphere. This reaction mixture was stirred at 0 ^{o}C for 72 h. The product was purified by precipitating from a tetrahydrofuran (THF) solution into methanol twice, and then dried under vacuum at room temperature for 72 h. This product was obtained in 33 % yield after the purification steps (fractional precipitation). The weight average molecular weight (M_w) and polydispersity index of the polymer measured using gel permeation chromatography (GPC) were 5,000 and 1.3, respectively. ^{1}H NMR of

poly[oxy(chloromethyl)ethylene] ($CDCl_3$, δ in ppm): 3.71 (m, 5H).

Preparation of poly[oxy[[2-(perfluorooctyl)ethyl]thiomethyl]ethylene]s (TP-Xs, where X is the mol % of monomeric units containing fluoroalkyl side group)

Comb-like fluorinated poly(oxyethylene)s were prepared by a polymer analogous reaction of poly[oxy(chloromethyl)ethylene] with sodium 1H,1H,2H,2H-perfluorodecane-1-thiolate, as reported previously.[40] Poly[oxy(chloromethyl)ethylene] (0.076 g, 0.82 mmol) was dissolved in an ionic liquid, 1-butyl-3-methyl-imidazolium chloride ([bmim][Cl]) (10 g), at 70 ^oC. This was followed by the addition of sodium *1H,1H,2H,2H*-perfluorodecane-1-thiolate, which had been prepared by a reaction of sodium with *1H,1H,2H,2H*-perfluorodecanethiol. Table 2.1 lists the mole percentage of sodium 1H,1H,2H,2H-perfluorodecane-1-thiolate used and the degree of substitution. The reaction mixture was stirred at 70 ^oC for 15 min and then poured into a water/methanol mixture. The precipitate was purified further by several precipitations from F113 into methanol. After further extraction with methanol for 12 h using a soxhlet extractor, the polymer was dried overnight under a higher vacuum. The product was obtained in above 80 % yield. The degree of substitution was calculated using the ^1H NMR results by comparing the multiplet at 2.39 ppm (2H) from the fluorinated alkyl side group and the multiplet at 3.64 (3H) from the backbone, which included the contribution of residual poly[oxy(chloromethyl)ethylene]. The M_w and polydispersity index of TP-100 were 17,600 and 1.3, respectively. ^1H NMR of TP-100 ($CDCl_3$/F113, δ in ppm): 2.39 (m, 2H),

2.73 (m, 2H), 2.81 (m, 2H), 3.64 (m, 3H).

Preparation of polymer thin films

Polymer thin films ($\leq$100 nm thick) were prepared by spin-coating a 1 wt% solution of the TP-Xs in F113 onto a silicon wafer at 3000 rpm for 30 sec using a spin-coater (Laurell model WS-400A-6NPP/LITE). The films were then dried in a vacuum oven for 24 h at room temperature. Annealing treatment was conducted through heating the polymer films at 60 ^{o}C for 2 h to compare the as-prepared and annealed films.

Analysis

The ^{1}H NMR spectra (500 MHz) were measured in either $CDCl_3$ or a $CDCl_3$/F113 mixture using Bruker, Avance 500. The M_w and polydispersity index were obtained on a Viscotek GPC using a diffractometer as the detector. THF and F113 were used as a solvent and monodisperse polystyrenes were used as the standards.

Differential scanning calorimetry (DSC, TA instruments 2920 differential scanning calorimeter) was carried out at heating and cooling rates of 5 ^{o}C min^{-1}. To eliminate the effect of the thermal history on the sample transitions, all samples were heated to 200 ^{o}C and held at that temperature for 5 min before cooling. The transition temperatures and enthalpy changes were obtained from the second heating scan.

The stylus surface roughness, R_a, was obtained by atomic force microscopy (AFM). The AFM observations were performed using an SPA300HV multifunction unit/SPI3800

probe station, Seiko Instruments Inc., Japan. The AFM images were obtained in tapping mode in air using a 20 μm x 20 μm scanner.

The molecular structure of polymer thin films could be characterized by combining the analysis of the near edge X-ray absorption fine structure (NEXAFS) and grazing incidence X-ray diffraction (GIXD). The NEXAFS experiments were conducted at the photoemission spectroscopy 2B1 beamline (beam size = 1 x 3 mm^2) at the Pohang Accelerator Laboratory, Korea. The C K-edge NEXAFS spectra were recorded in partial-electron-yield (PEY) mode. The degree of polarization of the X-ray was 0.85 and the entrance grid bias of -210 V was used. The soft X-ray incident angles were 20^o and 90^o for polarization dependence. The PEY signals were normalized by the incident beam intensity obtained from the photo yield of a clean silicon surface. Details of this technique are reported elsewhere.[41-44]

GIXD patterns were obtained using a high-power X-ray beam (photon flux ≈ 10^{11} photons s^{-1} $mrad^{-1}$ per 0.1%, beam size ≤0.5 mm^2) from a synchrotron radiation source (4C2 beamline, Pohang Accelerator Laboratory, Korea) at a wavelength λ = 1.3807 Å. The detection system was equipped with a two-dimensional X-ray detector (PI-SCX4300-165/2, Princeton Instrument). Details of the analytical methodology are reported elsewhere.[45,46]

The contact angles of the polymer thin film were determined using a Krüss DSA10 contact angle analyzer interfaced to a computer running drop shape analysis software. The advancing and receding contact angles were measured using drops of several liquids.

The contacting liquids (water, diiodomethane (DIM), ethylene glycol (EG), benzyl alcohol (BA), octane, decane, dodecane, and hexadecane) were of the highest purity available and used as received. The contact angles for each sample were measured a minimum of five times on independently prepared films and the average was used. The contact angle variability was within 1^{o} for all test liquids.

2.3. Results and Discussions

Figure 2.1 shows the synthetic route of the comb-like fluorinated poly(oxyethylene)s (TP-Xs, where X is the mol % of monomeric units containing fluoroalkyl side group) prepared by a polymer analogous reaction of poly[oxy(chloromethyl)ethylene] and sodium *1H,1H,2H,2H*-perfluorodecane-1-thiolate in an ionic liquid, 1-butyl-3-methyl-imidazolium chloride ([bmim][Cl]) as the reaction medium.[40] Table 2.1 lists the reaction conditions and degree of substitution. TP-Xs having high contents of fluoroalkyl side group could not be prepared using common organic solvents because the several highly fluorinated polymers including TP-Xs have very poor solubility in common organic solvents.[20,21,24,25,47] However, TP-Xs having high contents of fluoroalkyl side group could be prepared successfully when the ionic liquid, [bmim][Cl], was used as a reaction medium due to the ability of an ionic liquid to act as a reaction medium and catalyst, which can increase the degree of substitution in nucleophilic substitution reactions.[40,48-51] The content of fluoroalkyl side groups in TP-Xs could be controlled from 48 to 100 mol % by changing the poly[oxy(chloromethyl)ethylene] to sodium *1H,1H,2H,2H*-perfluorodecane-1-thiolate mole ratios from 0.55 to 1.20. The TP-Xs having lower content of fluoroalkyl side group such as 10 and 30 mol % were also synthesized with same procedures, however these polymers were not soluble in F113 and we could not obtain the films for the surface analysis. The casting solvent has been known to have negligible effect on tilt angles of fluoroalkyl groups,[18] while surface

morphology and contact angle values have been found to be affected by casting solvent.[9,18] Therefore we decided to use only one solvent (namely, F113) to prepare the films, and therefore the results from TP-Xs having fluoroalkyl side group less than 48 mol % were not included.

Figure 2.2 shows the DSC traces of the TP-Xs obtained from the second heating scan at a heating rate of 5 ^{o}C min^{-1}. Table 2.1 lists the transition temperatures and enthalpy changes. The glass transition temperature (T_g) increased with increasing content of the fluoroalkyl side groups, whereas no glass transition was observed for the polymers having ≥90 mol % of fluoroalkyl side group. A long and rigid fluoroalkyl side group might reduce the mobility of the polymer backbone, thereby increasing the T_g. An attempt was made to observe the T_g of TP-90 and TP-100 by quenching the melted samples in liquid nitrogen. However, the T_g was not observed. There are some reports that the glass transition of polymers having high content of fluoroalkyl side group is not easily detected from the DSC curves.[22,25,52] For all measured polymers, endothermic peaks were observed at approximately 90 ^{o}C, indicating the melting transition of the fluoroalkyl side group crystallites. The transition enthalpy change values increased with increasing content of fluoroalkyl side group, possibly due to the increased inter-side-chain interactions.[13,22]

"Annealed" films were prepared from "as-prepared" films by heating at 60 ^{o}C for 2 h to observe the effect of annealing treatment on the comb-like fluorinated poly(oxyethylene) thin films having different content of fluoroalkyl side group. The

annealing time was long enough to ensure thermodynamic equilibrium in the polymer thin films from a water contact angle experiment. Figure 2.3 shows the water advancing contact angle of the TP-Xs (48, 83, 100 mol %) according to the annealing treatment time. After a 1 h annealing treatment, all the measured films showed constant values. The stylus surface roughness, R_a, of the thin films obtained using AFM ranged from 1.1 to 5.7 nm (Table 2.2). These small R_a values indicate that the surface roughness has little effect on the contact angles and can be ignored in the contact angle measurements, i.e., a smooth surface (R_a <100 nm) does not affect the contact angle of the polymer films.[53]

NEXAFS and GIXD were used to further examine the effects of the content of fluoroalkyl side group and annealing treatment on the TP-Xs thin films. NEXAFS is a very useful technique for determining the molecular structural ordering near the outmost surface. Moreover, the average tilt angle of side group in the comb-like polymer thin films can be estimated.[17,18,22,43,44] Figure 2.4 shows the NEXAFS spectra of the C 1s edge of the annealed TP-100 thin film recorded at two incidence angles using PEY mode, such as 90^o (normal incidence) and 20^o (grazing incidence), respectively. Peaks corresponding to the 1s-σ^* transitions for the C-H, C-F and C-C bonds appeared at 288, 292, and 295 eV, respectively. Only the spectrum of the annealed TP-100 film is provided here as an example because all films showed similar results. The C-F bond intensity was larger at 90^o than at 20^o, whereas the C-C bond intensity showed an opposite behavior. This trend suggests that the fluoroalkyl side groups are oriented almost perpendicular to the film surface. The average tilt angles of the fluoroalkyl side group with the surface

normal were estimated from the calculation using the peak intensities of the C-F bonds at the grazing and normal incidence angles according to the procedure used by Ober *et al*.[17-19,22] As shown in Table 2.2 and Figure 2.5, the average tilt angles of all TP-Xs films lay in the range from 26^{o} to 33^{o}, which are larger than those of the semifluorinated self-assembled monolayer, but smaller than those of the comb-like fluorinated polymers reported by Ober *et al*.[17] and the fluorinated polystyrenes reported in our previous report.[22] This suggests that the fluoroalkyl side groups in the TP-Xs thin films have a more perpendicularly ordered structure to the film surface than the other fluorinated polymers, even though they are more tilted than the self-assembled monolayer.[17,22] The flexible oxyethylene backbone of TP-Xs could provide high mobility of fluoroalkyl side group to form well ordered structures almost perpendicular to the film surface. The content of fluoroalkyl side group had little effect on the average tilt angles, even though the average tilt angles appeared to increase with increasing content of fluoroalkyl side group from 58 to 100 mol %, while the changes are not much, if any. Furthermore, annealing treatment did not alter the average tilt angles significantly. Since the order parameter and tilt angle of the fluoroalkyl side group determined from NEXAFS represents an “average” value, it was not possible to distinguish between the case of all fluorinated groups being tilted homogeneously by the same angle and the case of disordered fluorinated groups with a wide distribution of tilt angles.[18,19,54] Moreover, the reported tilt angles, which were calculated using only two X-ray incident angles, do not take into account the effects of inelastic collisions of Auger electrons on the electron

yield and compositional depth profiles,[41,42] and are, therefore, only approximate values. Therefore, GIXD was carried out to distinguish and quantify the difference in molecular structural ordering and orientation of the TP-Xs thin films.

The two-dimensional GIXD patterns of the TP-Xs were recorded using a synchrotron X-ray beam at an incident angle of 0.17° (Figure 2.6). Table 2.2 lists the out-of-plane (small angle) and in-plane (wide angle) *d*-spacings obtained from the 2-D GIXD patterns. The out-of-plane diffraction patterns in the small angle region showed a series of peaks corresponding to the (00*h*) indices, indicating that the all thin films have lamellar structures oriented parallel to the film surface. The *d*-spacing of the (00*h*) reflection were similar to those of all films with lamellar thickness of 32 - 34 Å, and was approximately double that of the expected fluoroalkyl side group length assuming that the side groups are fully extended in the trans conformation.[13,22] The number of peaks from the out-of-plane scattering increased with increasing content of fluoroalkyl side group. For example, peaks for the (005) and (006) planes were observed from the as-prepared films containing >72 mol % of fluoroalkyl side group and annealed films containing >58 mol % of fluoroalkyl side group. Therefore, polymer films having more ordered lamellar structures were obtained by increasing content of fluoroalkyl side group and by annealing treatment, even though these thin films have similar *d*-spacings. In the case of TP-Xs having ≤72 mol % of fluoroalkyl side group, an additional lamellar structure with a slightly larger *d*-spacing than that of the original lamellar structure was observed after the annealing treatment. This additional lamellar structure appears to be generated by phase

separation between the hydrocarbon-rich and fluorocarbon-rich domains. Similar additional large lamellar structures were previously observed in comb-like polyacrylates having small contents of fluoroalkyl side group.[23]

The in-plane diffraction patterns shown in the wide-angle regions originated from the ordering of fluoroalkyl side group also showed a similar tendency. The intermolecular distances of the fluoroalkyl side group were similar (4.9 Å), which is the same as the intermolecular distance of the polytetrafluoroethylene crystals with the closest hexagonal packing of fluoroalkyl group.[55,56] This suggests that fluoroalkyl side groups on the polymer surface of both the as-prepared and annealed films have the closest hexagonal packing structures, regardless of the content of fluoroalkyl side group and annealing treatment. The flexible oxyethylene backbone in TP-Xs may provide high mobility of fluoroalkyl side group to form ordered packing structures, which in turn show hexagonally ordered fluoroalkyl side group structures despite their differences in the content of fluoroalkyl side group. On the other hand, the peaks from the out-of plane and in-plane scattering became sharper, and their intensities increased, with increasing content of fluoroalkyl side group. These GIXD patterns reveal that the fluoroalkyl side groups and lamellar structures were oriented perpendicular and parallel to the film surface, respectively, and more ordered molecular structures were obtained with increasing the content of fluoroalkyl side group, even though the out-of-plane and in-plane *d*-spacings were identical.

Paracrystalline structure analysis were carried out using the Hosemann paracrystal

model[29,30] to further quantify the difference in molecular structure of the TP-Xs. The Hosemann paracrystal model is considered the most suitable model to determine the polymer structures having lamellar structures.[13,14,31,32] The paracrystalline structure ordering, scattering unit number, and orientation could be derived from the 2-D GIXD patterns. Figure 2.7 shows a schematic diagram of the changes in the paracrystalline structure on the TP-Xs thin films. Paracrystalline structure ordering and scattering unit number were calculated using the reflection peaks in the small angle region, and a paracrystalline structure orientation was observed on the 2-D GIXD patterns.

For a paracrystalline system, the paracrystalline lattice factor $Z(s)$ of the hth-order reflection can be determined by the following:

$$Z(s) = Z(h) = [1-\exp(-4\pi^2 g^2 h^2)] \,/\, [(1-\exp(-2\pi^2 g^2 h^2))^2 + (4\sin^2 2\pi h)\, \exp(-2\pi^2 g^2 h^2)] \quad (2.1)$$

where s is the reciprocal lattice vector and g is the standard deviation of the Gaussian distribution divided by the average lattice vector $\tilde{a}$. g is a parameter used to evaluate the degree of paracrystalline structure disorder. The value of g is given experimentally by the following:

$$(\delta\beta)^2 = (1/\tilde{a}^2)[(1/N^2) + \pi^4 g^4 h^4] \quad (2.2)$$

where $\delta\beta$ is the integral breadth of a reflection, h is the scattering order, and N is the number of scattering units.[13,14] A linear relationship between $(\delta\beta)^2$ and h^4 could be obtained from the out-of-plane (001), (002), and (003) reflections of TP-Xs, and the g and N values were calculated using eq. 2.2.

As shown in Figure 2.8, the paracrystalline structure disorder parameter *g* decreased with increasing content of fluoroalkyl side group indicating that the level of paracrystalline structure ordering increases with increasing content of fluoroalkyl side group. In addition, the as-prepared films containing >72 mol % of fluoroalkyl side group and annealed films containing >58 mol % of fluoroalkyl side group have very low *g* values. However, the *g* values of the as-prepared films and annealed films with a same content of fluoroalkyl side groups were similar except for TP-48. The higher *g* value in TP-48 after annealing treatment might be caused by the additional lamellar structure produced after annealing treatment, as described above. Previously, the *g* values of poly(fluoroalkyl acrylate)[13] and poly(fluoroalkyl methacrylate)[14] films were found to decrease after annealing treatment, which is different from the TP-Xs in this study. Since the TP-Xs have a flexible oxyethylene backbone, highly ordered paracrystalline structures (smaller *g* values) could be prepared easily from the spin coating process. Therefore, the annealing treatment does not change the *g* values considerably. On the other hand, such highly ordered paracrystalline structures on the surface could not be obtained for the poly(fluoroalkyl acrylate)s and poly(fluoroalkyl methacrylate)s from the spin coating process because the backbone is not flexible enough, whereas the highly ordered surface structures were obtained after annealing treatment. Therefore, the *g* values of both the as-prepared and annealed TP-100 are similar to those of annealed poly(fluoroalkyl acrylate) and poly(fluoroalkyl methacrylate).[13,14] The *g* values of the TP-Xs indicate that the paracrystalline structure ordering of the as-prepared films containing >72 mol % of

fluoroalkyl side group and annealed films containing >58 mol % of fluoroalkyl side group are sufficiently high.

In the case of the *N* values meaning the number of scattering unit, the as-prepared films containing >72 mol % of fluoroalkyl side group and the annealed films containing >58 mol % of fluoroalkyl side group have larger scattering unit numbers than the other TP-Xs having lower content of fluoroalkyl side group. Therefore, the ordering and scattering unit number of the paracrystalline structure increase with increasing contents of fluoroalkyl side group. The scattering unit numbers show plateau values when the contents of side group are larger than 72 mol % in as-prepared films, and annealed films having >58 mol % content of fluoroalkyl side group show higher *N* values compared with the other films. After annealing treatment, paracrystalline structure ordering represented by the *g* value does not change significantly, whereas the scattering unit number increases, indicating that highly ordered paracrystalline structures have large “building blocks”.

The 2-D GIXD patterns can provide information on the orientation of paracrystalline structure. If the paracrystalline structures are randomly oriented within the film, the 2-D GIXD pattern consists of isotropic Debye-Scherrer diffraction rings rather than diffraction spots due to linkages of the diffraction spots from the same family of lattice planes.[31,32,44] As the paracrystalline structures are uniaxially oriented in a certain direction, the scattering ring patterns become weaker and form spots with a single orientation. As shown in Figure 2.6, all the as-prepared and annealed TP-48 films showed clear ring patterns both in the small and wide angle regions indicating that the orientation

of the paracrystalline structure is poor. As the content of fluoroalkyl side group was increased, their ring patterns became weaker and uniaxially oriented, but the ring patterns still remained, even for as-prepared TP-100. However, after the annealing treatment, polymer thin films having ≥58 mol % of fluoroalkyl side group showed sharp and condensed peak patterns indicating that the paracrystalline structures in the films are uniaxially oriented. Therefore, the annealed TP-Xs thin films containing ≥58 mol % of fluoroalkyl side group have highly ordered and uniaxially oriented paracrystalline structures with high scattering unit number.

The polymer surface properties, such as the surface energy and surface stability have been known to be related to the surface molecular structures.[7-16,22,24,38] In particular, highly ordered and uniaxially oriented paracrystalline structures with high scattering unit number (annealed TP-Xs containing ≥58 mol % of fluoroalkyl side group) were expected to show low surface energy and good surface stability. Taking the molecular structural analysis results into account, the surface energy and stability were further characterized in detail by the contact angle measurement. Table 2.3 shows the advancing contact angles and hysteresis of the TP-Xs thin films using various test liquids. The advancing and receding contact angles were measured using 8 kinds of liquid from water, with the highest surface tension, to octane with the lowest. The contact angle hysteresis (*H*) is the difference between the advancing and receding contact angle values. The correlation between the contact angle and surface energy is still controversial and none of the methods proposed are generally accepted.[57,58] Normally, two or three test liquids are

used for the contact angle measurements, which are then used to obtain the surface energy. In these cases, the surface energies vary according to the types of liquid used for the measurements.[22,58] The acid-base approach involves three different surface tension components, i.e., the Lifshitz-van der Waals dispersive component, γ^{LW}, polar Lewis acid component, γ^{+}, and polar Lewis base component, γ^{-} , such that the total surface energy, γ^{total}, can be given by the following equation:

$$\gamma_i^{total} = \gamma_i^{LW} + 2(\gamma_i^{+} \gamma_i^{-})^{1/2} \qquad (2.3)$$

which leads to a Young's equation of the following form:

$$\gamma_l(1 + \cos\theta) = 2(\gamma_l^{LW}\gamma_s^{LW})^{1/2} + 2(\gamma_l^{+}\gamma_s^{-})^{1/2} + 2(\gamma_l^{-}\gamma_s^{+})^{1/2} \qquad (2.4)$$

This approach requires contact angle values from at least 3 test liquids. The trend of surface energies shows that annealed TP-Xs films containing ≥58 mol % of fluoroalkyl side group have lower surface energies than the other films, even though these values vary from 8.54 to 10.97 mJ/m^2 when different liquid systems were used (Table 2.S1). These different values were generated by a liquid-surface interaction and/or surface reconstruction depending on the polarity of the test liquid.[22,57-59] To estimate the intrinsic surface energy of a solid, we adopted a equation of state approach that Kwok and Neumann derived an expression using eq. 2.5. On the other hand, with the other commonly used methods, only one intrinsic surface energy can be obtained by the equation of state approach using eq. 2.5, because this approach is based on the equation of state relating the surface energy of a liquid (γ_{lv}) and solid (γ_{sv}).[58,59]

$$\cos\theta = -1 + 2(\gamma_{sv} / \gamma_{lv})^{1/2} (1 - \beta_I(\gamma_{lv} - \gamma_{sv})^2) \qquad (2.5)$$

The intrinsic surface energy of solid was evaluated by curve fitting method using the 8 kinds of test liquids. The correlation between surface tension of test liquids and contact angles on each surface determined the intrinsic surface energy of polymer films. The γ_{sv} value of the polymer film determined using γ_{lv} and the contact angle (θ), from the line of best fit in eq. 2.5. β_1 is a constant value, 0.0001057.[58] Figure 2.9 show the calculated surface energies. The surface energies of the annealed films are smaller than those of the as-prepared films when they have the same fluoroalkyl side group content. In addition, the surface energy generally decreases with increasing content of fluoroalkyl side group. In particular, the annealed TP-Xs containing ≥58 mol % of fluoroalkyl side groups have lower surface energies than the other TP-Xs in the range of 9.9 - 10.2 mJ m^{-2}. This behavior follows to some degree the changes in the number of scattering units, *N* value, and paracrystalline structure orientation measured from the 2-D GIXD patterns. After annealing treatment, the *N* values of the TP-Xs containing ≥58 mol % of fluoroalkyl side group increased and the GIXD patterns become sharper without ring patterns. The as-prepared films containing ≥72 mol % of fluoroalkyl side group having less sharper GIXD patterns with some ring patterns have larger surface energies than the annealed films containing ≥58 mol % of fluoroalkyl side group (Figure 2.6), even though they have similar paracrystalline structure ordering, as represented by the *g* values. The surface energy behavior does not follow the changes in the average tilt angle, lamellar thickness, and the inter-chain distance of fluoroalkyl side group. These values did not change significantly after annealing treatment and are less affected by the content of fluoroalkyl

side group. As mentioned in previously, the *g* values of all TP-Xs containing ≥58 mol % of fluoroalkyl side groups are close to those of other annealed comb-like fluorinated polymers with highly ordered structures. The inter-chain distance of the fluoroalkyl side group of TP-Xs are the same as the intermolecular distance of the polytetrafluoroethylene crystals with the closest hexagonal packing of fluoroalkyl group, and the tilt angles of the TP-Xs are even smaller than those of the other comb-like fluorinated polymers.[13,14,17,55,56] Therefore, these TP-Xs values are already the minimum values for fluorinated polymers. Hence, further annealing treatment cannot lower them further. However, the *N* values and paracrystalline structure orientation measured from 2-D GIXD patterns change after annealing treatment. Therefore, a further decrease in surface energy with increasing content of fluoroalkyl side group of the TP-Xs and after annealing treatment could be correlated with the *N* values and paracrystalline structure orientation measured from the 2-D GIXD patterns. The surface energies of TP-Xs are affected by paracrystalline structure ordering, orientation and scattering unit number. In the case of annealed TP-48 and as-prepared TP-100 films, the as-prepared TP-100 film shows smaller surface energy value than the annealed TP-48 one despite of its lower scattering unit number. This phenomenon could be explained by the *g* value (paracrystalline ordering) trend. The *g* value of the annealed TP-48 is larger than that of the as-prepared TP-100. Large *g* value means a poor paracrystalline structure ordering. TP-Xs having > 58 mol% of fluoroalkyl side groups show very small g values. However, TP-48 shows larger g value than other TP-Xs, so it has larger surface energy value. This

result indicates that both small *g* and large *N* values are required for the surfaces to have the small surface energy. If the *g* values are sufficiently small, then the *N* value and paracrystalline orientation become important parts to determine the surface energy as the annealed TP-Xs films having ≥58 mol % of fluoroalkyl side group.

The annealed TP-Xs films having ≥58 mol % of fluoroalkyl side group also showed high surface stability against the polar test liquids during the contact angle experiment. As shown in Table 2.3, some of the contact angles are not available from ethylene glycol (EG) or benzyl alcohol (BA). The contact angles of EG could not be obtained on all the as-prepared films and annealed TP-48 because these liquids smeared into these polymer films, possibly due to the partial miscibility of EG with these polymers films. However, the contact angles of EG on the annealed TP-Xs thin films, which have highly ordered and uniaxially oriented paracrystalline structures with high scattering unit number, could be measured due to the improved surface structural stability. In the case of BA, although the stability difference is not as significant as in the case of EG, BA was found to smear in polymer films containing lower contents of fluoroalkyl side groups, such as as-prepared TP-48 and TP-58 and annealed TP-48. This stability also follows the changes in surface energy, *N* values, and paracrystalline structure orientation measured from the 2-D GIXD patterns.

2.4. Conclusions

Comb-like fluorinated poly(oxyethylene)s having different content of fluoroalkyl side group were characterized by NEXAFS, GIXD, and contact angle measurements to correlate the surface properties with their molecular structures. There was no strong correlation between the contents of fluoroalkyl side groups and the tilt angle of the side chains. The *d*-spacing of all the comb-like fluorinated poly(oxyethylene)s was very similar, even though the polymers have different contents of fluoroalkyl side groups. Furthermore, these values did not change after annealing treatment. The paracrystalline structure ordering represented by the *g* value also did not change after annealing treatment, whereas the *g* values of the as-prepared films having ≥72 mol % of fluoroalkyl side group and the annealed films having ≥58 mol % of fluoroalkyl side group were smaller (better paracrystalline structure ordering) than those with a smaller amount of fluoroalkyl side groups. The *d*-spacing values, *g* values, and tilt angles of the comb-like fluorinated poly(oxyethylene)s were close to or even lower than the other fluorinated polymers. Therefore, further changes in the tilt angles, *d*-spacing values, and g values were not possible, so they do not represent the changes in the surface energy of the comb-like fluorinated poly(oxyethylene)s according the content of the fluoroalkyl side group and after annealing treatment. However, the surface properties follow the changes in the number of scattering units, which are represented by the *N* value and paracrystalline structure orientation measured from the 2-D GIXD patterns. For example, annealed

polymer thin films having ≥58 mol % of fluoroalkyl side group showed uniaxially oriented paracrystalline structures with a large *N* value. In addition, these films showed high surface stability with a very low surface energy in the range of 9.9 -10.2 mJ/m^2 calculated using the equation of state approach. On the other hand, the surface energy of the annealed polymer film having <58 mol % of fluoroalkyl side group and those of all the as-prepared films having less oriented paracrystalline structures and smaller *N* value are larger than 10.5 mJ/m^2. Therefore, the orientation of the paracrystalline structure and *N* value are important parameters to have a strong correlation with the surface energy of comb-like fluorinated poly(oxyethylene)s. This is believed to be the first report to show a clear relationship between the surface properties and the orientation of the paracrystalline structure and scattering unit number.

Table 2.1 Reaction conditions,[a] degree of substitution and thermal properties of TP-Xs

	Sodium perfluorodecane thiolate (mol %)	Degree of substitution (mol %)	T_g (°C)	Transition, °C (ΔH, mJ/mol)
TP-48	55	48	41.3	90.4 (4.1)
TP-58	65	58	41.8	90.3 (4.2)
TP-72	75	72	46.4	87.8 (14.1)
TP-83	85	83	54.3	86.9 (19.2)
TP-90	100	90		90.2 (26.6)
TP-100	120	100		91.8 (50.1)

[a]Reaction temperature and time were 70 °C and 15 min, respectively.

Table 2.2 AFM, GIXD and NEXAFS results of TP-Xs.

		AFM result	NEXAFS results			GIXD results	
		R_a (nm)	$S_{C\text{-}F}$[a]	$S_{F\text{-}helix}$[b]	Tilt angle (o)[c]	Small angle *d*-spacing (Å)[d]	Wide angle *d*-spacing (Å)[e]
As-prepared films	TP-48	1.2	-0.2869	0.5738	32.21	33.6, 17.6, 11.6	4.94
	TP-58	1.3	-0.3572	0.7144	25.86	34.3, 17.8, 11.8	4.85
	TP-72	1.5	-0.3472	0.6944	26.82	34.4, 17.6, 11.8, 5.7	4.92
	TP-83	1.1	-0.3192	0.6384	29.40	32.6, 16.3, 11.0, 6.6, 5.7	4.90
	TP-90	1.6	-0.3297	0.6594	28.46	32.9, 16.9, 11.3, 6.8, 5.7	4.93
	TP-100	1.2	-0.3145	0.6290	29.82	32.1, 16.5, 11.0, 6.6, 5.5	4.90
Annealed films	TP-48	3.5	-0.2835	0.5670	32.50	32.9, 16.9, 11.3 (38.4, 19.5, 13.2)[f]	4.92
	TP-58	5.7	-0.3499	0.6998	26.57	32.3, 16.7, 11.3, 5.8 (38.6, 19.5, 13.2)[f]	4.96
	TP-72	3.4	-0.3347	0.6694	28.00	34.4, 17.2, 11.5, 6.8, 5.7 (38.2, 19.3, 12.9)[f]	4.93
	TP-83	2.1	-0.3231	0.6462	29.05	32.3, 16.5, 11.2, 6.8, 5.8	4.98
	TP-90	1.6	-0.2814	0.5628	32.67	32.3, 16.5, 11.2, 6.7, 5.6	4.96
	TP-100	1.5	-0.3079	0.6158	30.41	32.1, 16.3, 11.0, 6.6, 5.6	4.96

[a]Surface orientational parameter of C-F bonds.

[b]Surface orientational parameter of fluoroalkyl helix.

[c]Tilt angle of fluoroalkyl helix to the surface normal.

[d]A series of *d*-spacings corresponding to the 001, 002, 003, 005, and 006 indices of lamellar thickness.

[e]*d*-Spacings representing the distance between the fluorinated alkyl side chains.

[f]Additional lamellar structure.

Table 2.3 Advancing contact angles and hysteresis of TP-Xs using various test liquids.

		Contact angle, θ, (hysteresis) [deg]							
		Water	DIM[a]	EG[b]	BA[c]	Octane	Decane	Dodecane	Hexadecane
As-prepared films	TP-48	120.1 (20.7)	96.7 (26.5)	[d]	[d]	70.9 (13.5)	75.4 (10.7)	78.1 (11.5)	81.0 (9.8)
	TP-58	123.1 (24)	96.9 (27.2)	[d]	[d]	71.0 (18.6)	75.4 (11.6)	78.2 (15.4)	81.7 (13)
	TP-72	124.3 (24.2)	96.9 (25.6)	[d]	91.7 (22.2)	71.7 (14.5)	75.9 (12.6)	78.9 (16.5)	81.8 (14.1)
	TP-83	124.7 (25.3)	96.7 (26.4)	[d]	93.4 (30.6)	71.7 (16.6)	76.5 (14.1)	78.8 (17.1)	83.0 (16.8)
	TP-90	125.3 (24.5)	97.9 (28.3)	[d]	92.8 (26.2)	71.8 (12.7)	76.3 (14.2)	78.8 (17.8)	82.1 (14.9)
	TP-100	125.9 (26.3)	97.3 (27.1)	[d]	91.5 (22.3)	71.3 (11)	75.2 (14.1)	78.3 (17.5)	81.9 (16.5)
Annealed films	TP-48	122.3 (21.6)	97.9 (23)	[d]	[d]	71.1 (10.5)	75.4 (8)	78.8 (10.6)	81.3 (13.2)
	TP-58	122.0 (26)	100.6 (33.1)	105.4 (27.4)	94.6 (42.3)	72.7 (12.4)	77.3 (10.2)	81.6 (11.8)	85.6 (10.1)
	TP-72	123.4 (22)	100.4 (14.5)	105.2 (27)	95.5 (33.9)	73.2 (12)	77.4 (7.5)	81.2 (8.7)	85.2 (8.8)
	TP-83	123.5 (23.1)	100.4 (27.2)	105.1 (32)	93.3 (31)	72.4 (11.2)	76.9 (11.3)	80.0 (13.4)	83.8 (16.2)
	TP-90	123.0 (24.6)	100.4 (16.1)	104.4 (26.4)	93.9 (30.4)	72.4 (9.4)	77.0 (7)	80.4 (7.8)	85.1 (10.8)
	TP-100	123.7 (24.1)	100.2 (15.4)	104.6 (27.2)	94.0 (26.5)	72.9 (9.5)	77.1 (6.6)	80.9 (7.7)	84.9 (9.6)

[a]Diiodomethane. [b]Ethylene glycol. [c]Benzyl alcohol.

[d]Measurement was not possible because polymer film is partially soluble in EG and BA.

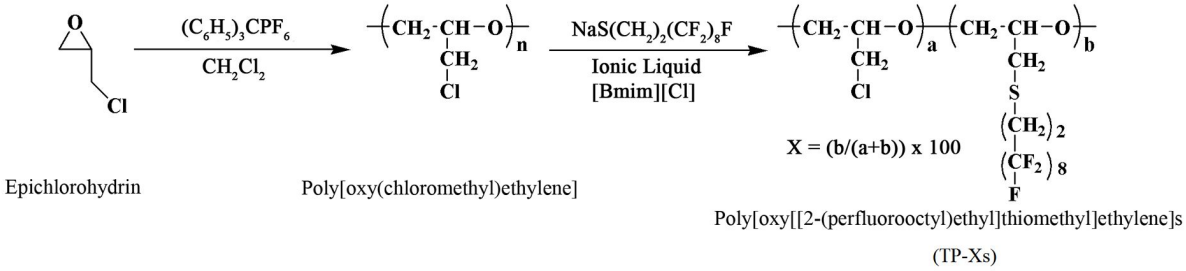

Figure 2.1. Synthetic route for TP-Xs.

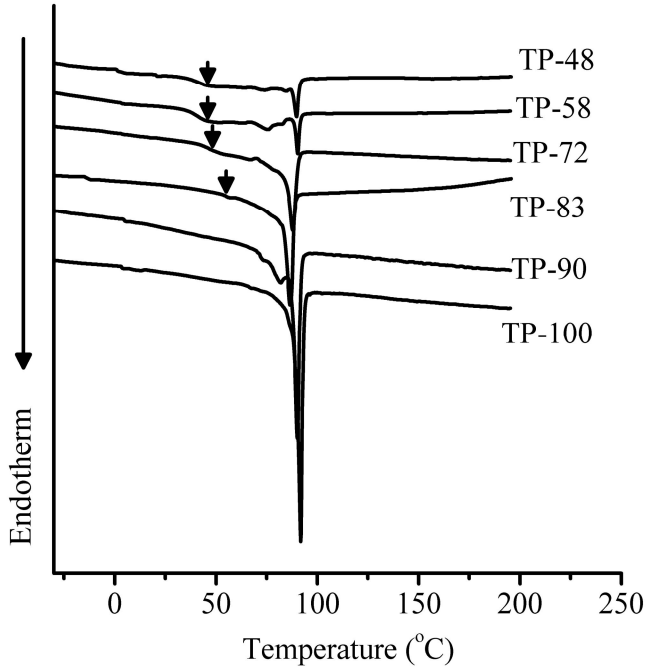

Figure 2.2. DSC curves of TP-Xs (The black arrows indicate the glass transition temperature).

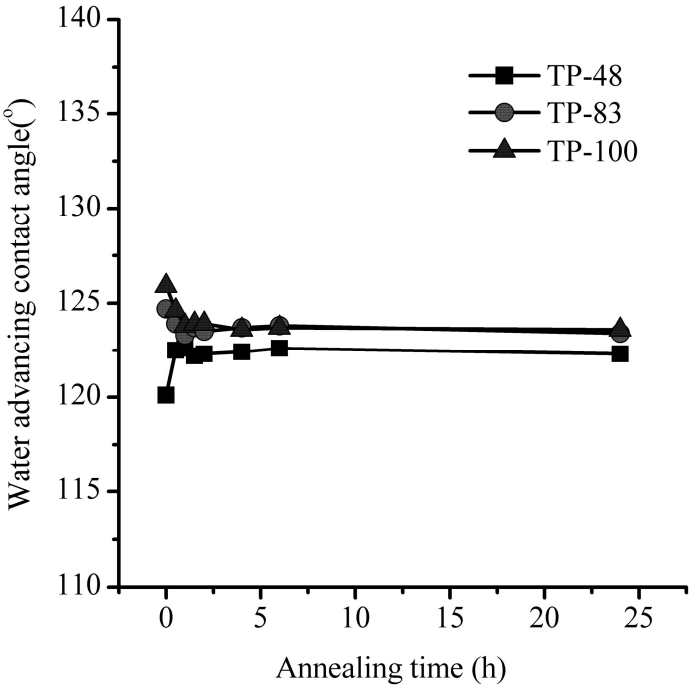

Figure 2.3. The water contact angles of TP-48, TP-83, and TP-100 according to annealing time. The solid lines are guides to the eye.

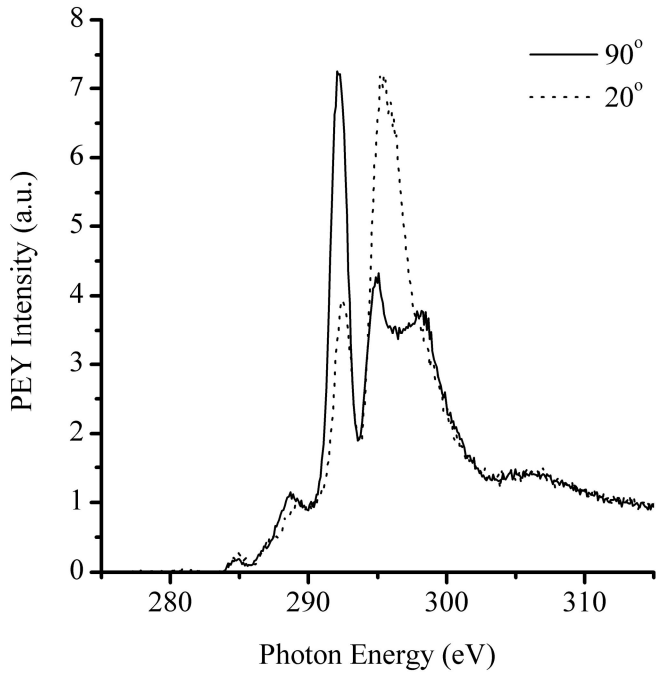

Figure 2.4. PEY NEXAFS spectra from the annealed TP-100 thin film at two different incidence angles.

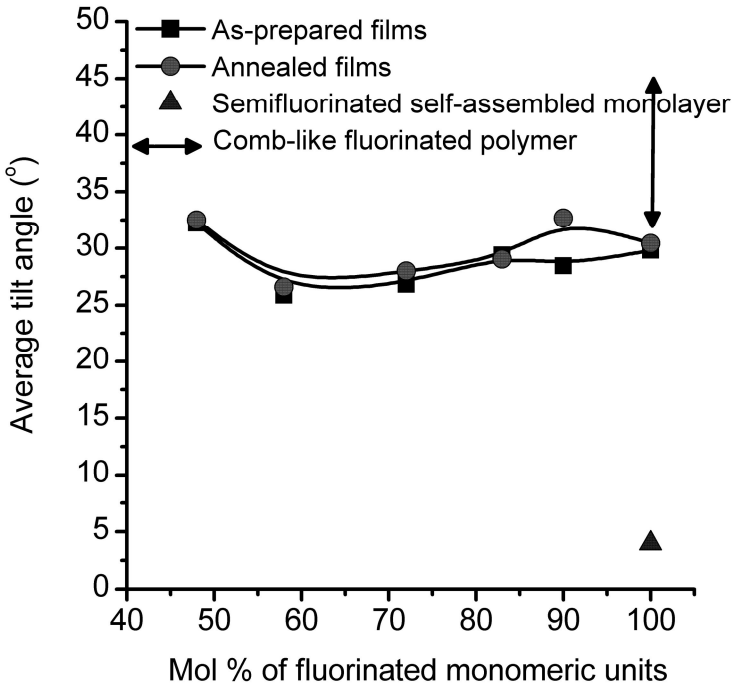

Figure 2.5 Average tilt angles of fluoroalkyl side group with the surface normal. Semifluorinated self-assembly monolayer and comb-like fluorinated polymer values were described in ref 17 and 22. The solid lines are guides to the eye.

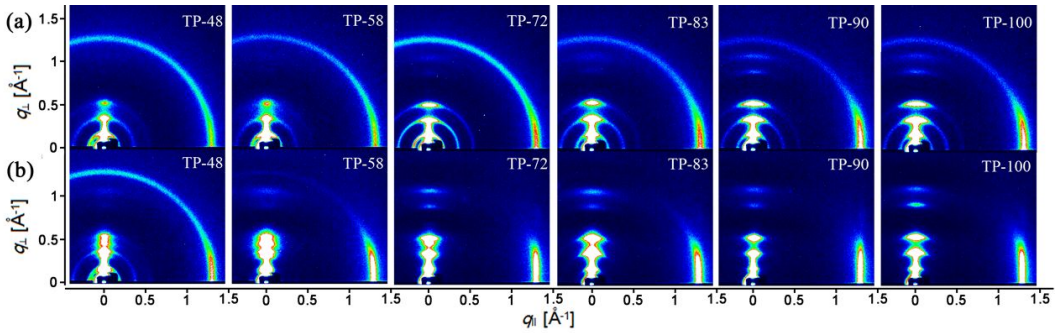

Figure 2.6 Two-dimensional GIXD patterns of the (a) as-prepared films and (b) annealed films.

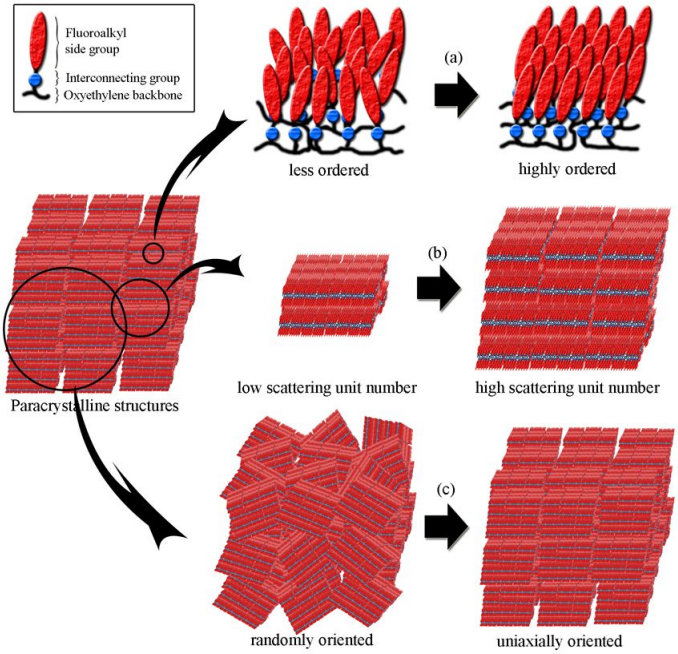

Figure 2.7. Schematic diagram for the changes of paracrystalline structure (a) ordering, (b) scattering unit number and (c) orientation.

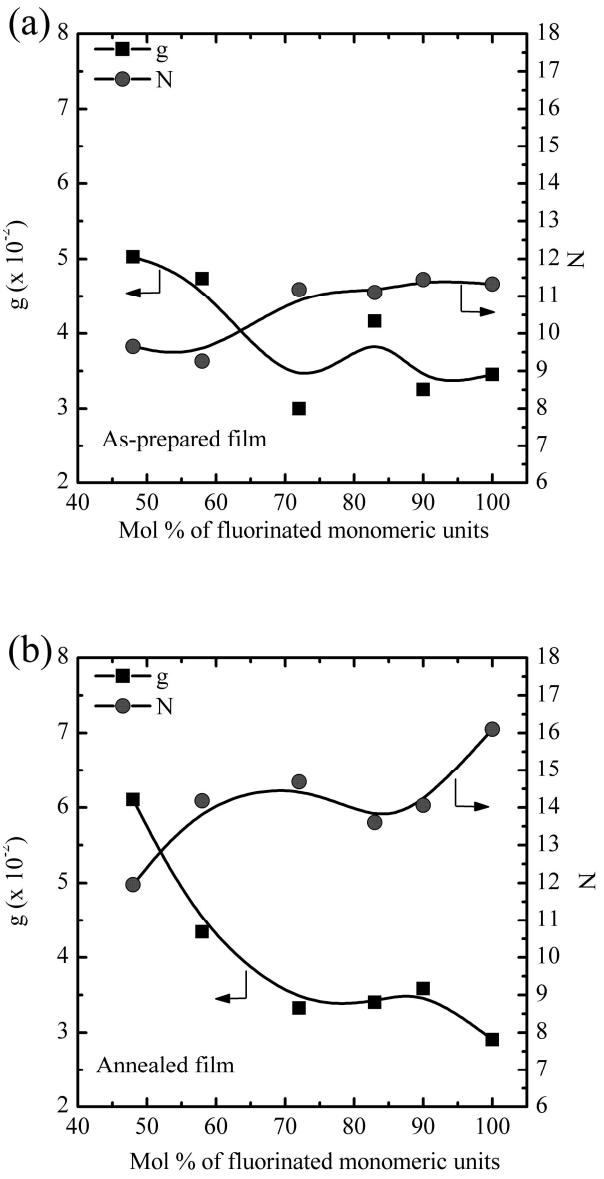

Figure 2.8. Paracrystalline structure disorder parameter (*g*) and number of scattering unit (*N*) values for (a) as-prepared films and (b) annealed films. The solid lines are guides to the eye.

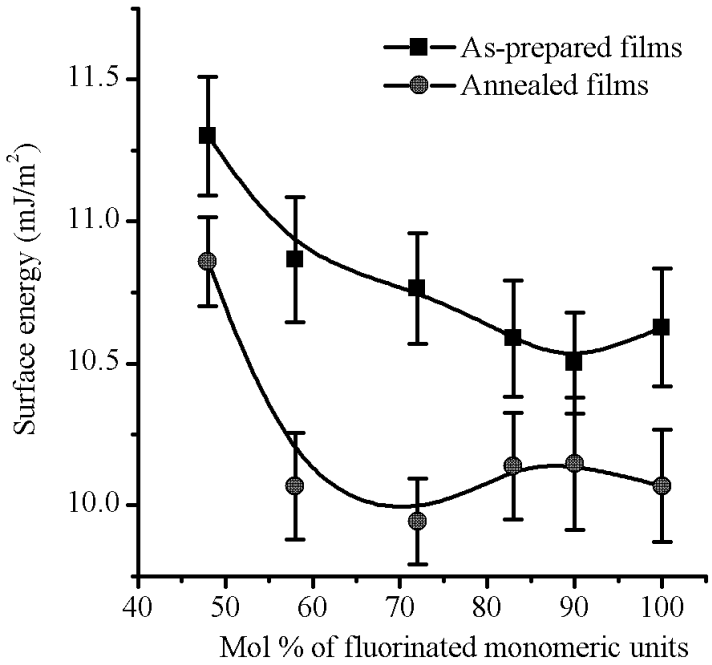

Figure 2.9. Surface energy obtained from equation of state approach of the TP-Xs. The solid lines are guides to the eye.

2.5. References

[1] Hougham, G. *In Fluoropolymers*; Hougham, G., et al., Eds.; Plenum Press: New York, 1999.

[2] Scheirs, J., Ed. *Modern Fluoropolymers: High Performance Polymers for Diverse Applications*; Wiley: New York, 1997.

[3] Lee, S.; Park, J.-S.; Lee, T. R. *Langmuir* **2008,** 24, 4817.

[4] Schmidt, D. L.; Coburn, C. E.; Dekoven, B. M.; Potter, G. E.; Meyers, G. F.; Fisher, D. A. *Nature* **1994**, 368, 39.

[5] Bryan-Brown, G. P.; Wood, E. L.; Sage, I. C. *Nature* **1999**, 399, 338.

[6] Ober, C. K.; Gabor, A. H.; Gallagher-Wetmore, P.; Allen, R. D. *Adv. Mater.* **1997**, 9, 1039.

[7] Tsibouklis, J.; Nevell, T. G. *Adv. Mater.* **2003**, 15, 647.

[8] Tsibouklis, J.; Graham, P.; Eaton, P. J.; Smith, J. R.; Nevell, T. G.; Smart, J. D.; Ewen, R. J. *Macromolecules* **2000**, 33, 8460.

[9] Urushihara, Y.; Nishino, T. *Langmuir* **2005**, 21, 2614.

[10] Park, I. J.; Lee, S. B.; Choi, C. K. *Macromolecules* **1998,** 31, 7555.

[11] Hirao, A.; Sugiyama, K.; Yokoyama, H. *Prog. Polym. Sci.* **2007**, 32, 1393.

[12] Matsunaga, M.; Suzuki, T.; Yamamoto, K.; Hasegawa, T. *Macromolecules* **2008,** 41, 5780.

[13] Honda, K.; Morita, M.; Otsuka, H.; Takahara, A. *Macromolecules* **2005**, 38, 5699.

[14] Honda, K.; Morita, M.; Sakata, O.; Sasaki, S.; Takahara, A. *Macromolecules* **2010**, 43, 454.

[15] Yamaguchi, H.; Honda, K.; Kobayashi, M.; Morita, M.; Masunaga, H.; Sakata, O.; Sasaki, S.; Takahara, A. *Polymer Journal* **2008**, 40, 854.

[16] Wang, J.; Mao, G.; Ober, C. K.; Kramer, E. J. *Macromolecules* **1997**, 30, 1906.

[17] Genzer, J.; Sivaniah, E.; Kramer, E. J.; Wang, J.; Körner, H.; Xiang, M.; Char, K.; Ober, C. K.; DeKoven, B. M.; Bubeck, R. A.; Chaudhury, M. K.; Sambasivan, S.; Fischer, D. A. *Macromolecules* **2000,** 33, 1882.

[18] Genzer, J.; Sivaniah, E.; Kramer, E. J.; Wang, J.; Xiang, M.; Char, K.; Ober, C. K.; Bubeck, R. A.; Fischer, D. A.; Graupe, M.; Colorado, R. Jr.; Shmakova, O. E.; Lee, T. R. *Macromolecules* **2000**, 33, 6068.

[19] Li, X.; Andruzzi, L.; Chiellini, E.; Galli, G.; Ober, C. K.; Hexemer, A.; Kramer, E. J.; Fischer, D. A. *Macromolecules* **2002**, 35, 8078.

[20] Krishnan, S.; Ayothi, R.; Hexemer, A.; Finlay, J. A.; Sohn, K. E.; Perry, R.; Ober, C. K.; Kramer, E. J.; Callow, M. E.; Callow, J. A.; Fischer, D. A. *Langmuir* **2006**, 22, 5075.

[21] Busch, P.; Krishnan, S.; Paik, M.; Toombes, G. E. S.; Smilgies, D.-M.; Gruner, S. M.; Ober, C. K. *Macromolecules* **2007**, 40, 81.

[22] Kim, B. G.; Chung, J.-S.; Sohn, E.-H.; Kwak, S.-Y.; Lee, J.-C. *Macromolecules* **2009,** 42, 3333.

[23] de Crevoisier, G.; Fabre, P.; Leibler, L.; Tence-Girault, S.; Corpart, J. M.

Macromolecules **2002**, 35, 3880.

[24] Kim, B. G.; Sohn, E.-H.; Cho, K.; Lee, J.-C. *Eur. Polym. J.* **2008**, 44, 2912.

[25] Paik, M. Y.; Krishnan, S.; You, F.; Li, X.; Hexemer, A.; Ando, Y.; Kang, S. H.; Fischer, D. A.; Kramer, E. J.; Ober, C. K. *Langmuir* **2007**, 23, 5110.

[26] Liu, Y.; Nagle, J. F. *Phys. Rev. E.* **2004**, 69, 040901.

[27] Pabst, G.; Rappaolt, M.; Amenitsch, H.; Laggner, P. *Phys. Rev. E.* **2000**, 62, 4000.

[28] Yakabe, H.; Sasaki, S.; Sakata, O.; Takahara, A.; Kajiyama, T. *Macromolecules* **2003,** 36, 5905.

[29] Lindenmeyer, P. H.; Hosemann, R. *J. Appl. Phys.* **1963**, 34, 42.

[30] Hosemann, R.; Hindeleh, A. M. *J. Macromol. Sci. Phys.* **1995**, B34, 327.

[31] Yoon, J.; Jin, K. S.; Kim, H. C.; Kim, G.; Heo, K.; Jin, S.; Kim, J.; Kim, K.-W.; Ree, M. *J. Appl. Cryst.* **2007**, 40, 476.

[32] Yoon, J.; Lee, S. W.; Choi, S.; Heo, K.; Jin, K. S.; Jin, S.; Kim, G.; Kim, J.; Kim, K.-W.; Kim, H.; Ree, M. *J. Phys. Chem. B.* **2008**, 112, 5338.

[33] Lee, J.-C.; Litt, M. H.; Rogers, C. E. *Macromolecules* **1997**, 30, 3766.

[34] Lee, J.-C.; Litt, M. H.; Rogers, C. E. *Macromolecules* **1998**, 31, 2440.

[35] Lee, J.-C.; Oh, K.; Lee, H. B.; Kim, Y. G.; Jho, J. Y.; Kwak, S.-Y.; Park, S.-Y.; Farmer, B. L. *Macromol. Rapid commun.* **2001**, 22, 815.

[36] Lee, J.-C.; Lim, M.-Y.; Oh, K.; Lee, H. B.; Kim, Y. G.; Park, S.-Y.; Farmer, B. L. *Polymer* **2002**, 43, 7051.

[37] Lee, J.-C.; Han, S.-H.; Cha, S. H.; Park, S.-Y.; Farmer, B. L. *Polymer* **2003**, 44,

7413.

[38] Kim, B. G.; Sohn, E.-H.; Lee, J.-C. *Macromol. Chem. Phys.* **2007**, 208, 1011.

[39] Kim, B. G.; Moon, J.-K.; Sohn, E.-H.; Lee, J.-C. *Macromol. Res.* **2008**, 16, 36.

[40] Kim, B. G.; Sohn, E.-H.; Chung, J.-S.; Kwak, S.-Y.; Lee, J.-C. *J. Appl. Polym. Sci.* 2009, 114, 132.

[41] Sohn, K. E.; Dimitriou, M. D.; Genzer, J.; Fischer, D. A.; Hawker, C. J.; Kramer, E. J. *Langmuir* **2009,** 25, 6341.

[42] Krishnan, S.; Paik, M. Y.; Ober, C. K.; Martinelli, E.; Galli, G.; Sohn, K. E.; Kramer, E. J.; Fischer, D. A. *Macromolecules* **2010,** 43, 4733.

[43] Stohr, J. *NEXAFS spectroscopy*; Springer series in surface sciences 25; Springer-Verlag: Berlin, 1992.

[44] Zubavichus, Y.; Shaporenko, A.; Grunze, M.; Zharnikov, M. *J. Phys. Chem. B.* **2006,** 110, 3420.

[45] Lee, B.; Park, Y.-H.; Hwang, Y.-T.; Oh, W.; Yoon, J.; Ree, M. *Nat. Mater.* **2005**, 4, 147.

[46] Yoon, J.; Kim, K.-W.; Kim, J.; Heo, K.; Jin, K. S.; Jin, S.; Shin, T. J.; Lee, B.; Rho, Y.; Ahn, B.; Ree. M. *Macromol. Res.* **2008**, 16, 575.

[47] Anton, D. *Adv. Mater.* **1998,** 10, 1197.

[48] Ranu, B. C.; Jana, R. *Adv. Synth. Catal.* **2005**, 347, 1811.

[49] Kim, D. W.; Song, C. E.; Chi, D. Y. *J. Am. Chem. Soc.* **2002**, 124, 10278.

[50] Lourenco, N. M. T.; Afonso, C. A. M. *Tetrahedron* **2003**, 59, 789.

[51] Lee, S.; Zhang, Y. J.; Piao, J. Y.; Yoon, H.; Song, C. E.; Choi, J. H.; Hong, J. *Chem. Commun.* **2003,** 2624.

[52] Shimizu, T.; Tanaka, Y.; Kutsumizu, S.; Yano, S. *Macromolecules* **1996**, 29, 156.

[53] Busscher, H. J.; van Pelt, A. W. J.; de Boer, P.; de Jong, H. P.; Arends, J. J. *Colloid Surface* **1984**, 9, 319.

[54] Genzer, J.; Efimenko, K.; Fischer, D. A. *Langmuir* **2006**, 22, 8532.

[55] Volkov, V.; Plate, N.; Takahara, A.; Kajiyama, T.; Amaya, N.; Murata, Y. *Polymer* **1992**, 33, 1316.

[56] Corpart, J. M.; Girault, S.; Juhue, D. *Langmuir* **2001**, 17, 7237.

[57] Martinelli, E.; Menghetti, S.; Galli, G.; Glisenti, A.; Krishnan, S.; Paik, M. Y.; Ober, C. K.; Smilgies, D.-M.; Fischer, D. A. *J. Polym. Sci. Part. A: Polym. Chem.* **2009**, 47, 267.

[58] Kwok, D. Y.; Neumann, A. W. *Adv. Colloid interface Sci.* **1999**, 81, 167.

[59] Tavana, H.; Neumann, A. W. *Adv. Colloid interface Sci.* **2007**, 132, 1.

Chapter 3

Silver-Perfluorodecanethiolate Complexes Having Superhydrophobic, Antifouling, Antibacterial Properties

3.1. Introduction

Fluorinated compounds are an obvious choice for a range of applications, such as coatings, electronic and medical materials to improve their performance and functionality [1-3]. With the rapid progress of fluorinated compounds in recent years, many attempts have been made to obtain superhydrophobic properties using these materials [4-6]. Owing to the large number of applications, such as water repellent materials, self-cleaning surfaces, controlling cell adhesion, and reducing fluid resistances, the superhydrophobic property is currently under a spotlight [7-13]. Superhydrophobic materials can be obtained by making micro/nano-sized structures using hydrophobic materials and these micro-/nano-sized structures have been created by lithography, electrochemical deposition or electrospinning process [14-18]. Since these processes are normally tedious and time consuming, it is very desirable to develop a simpler process for the preparation of superhydrophobic surfaces.

Metal-thiolate complexes have been well documented in the literature and their detail characteristics have been elucidated by many research groups [19-23]. The unique characteristics of metal-thiolate complexes are essentially dependent on their structures. For example, metal-alkanethiolate complexes have well developed bilayer structures with all-trans chain conformations. These complexes can be used as precursor materials for the synthesis of metal nanomaterials [22,24-26]. Recently, the metal-thiolate complexes were used to fabricate the superhydrophobic surfaces [27,28]. Owing to the well developed bilayer structure, metal-alkanethiolate complexes show hierarchical micro-/nano-sized

structures, then superhydrophobic properties can be obtained.

This paper reports the facile and simple preparation of silver-perfluorodecanethiolate complexes (AgSF, Figure. 3.1) having wire shape structure. They exhibited superhydrophobic and antifouling properties due to the highly fluorinated hierarchical structure. When irradiated with UV-light, silver nanoparticles were formed on the surface of wires and showed antibacterial properties. Although there are a few studies on the metal-thiolate complexes with fluorinated groups [29-33], to the best of our knowledge, there are no reports on the antifouling and antibacterial properties using the metal-thiolate complexes.

3.2. Experimental

Materials

Silver nitrate ($AgNO_3$), 1*H*,1*H*,2*H*,2*H*-perfluorodecanethiol (PFDT), and polystyrene were purchased from Sigma-Aldrich Co. and triethylamine (TEA) was supplied by TCI. *Pseudomonas aeruginosa* PAO1 tagged with green fluorescent protein (PAO1) was obtained from the Center for Biofilm Engineering (Montana State University, USA). All reagents and solvents were used as received.

Synthesis and sample preparation

AgSF was prepared by a reaction of $AgNO_3$ with PFDT. The molar ratio of $AgNO_3$ to PFDT was varied from 10/1 to 1/10 by changing the amount of $AgNO_3$ solution to observe the shape change of the synthesized AgSF. The synthetic procedure is exemplified in the case of AgSF having wire shape structure. A solution of PFDT (960 mg, 2 mmol) and TEA (203 mg, 2 mmol) in ethanol (20 ml) was mixed with a solution of $AgNO_3$ (170 mg, 1 mmol) in ethanol (20 ml) at room temperature. A white precipitate formed immediately. After 24 h, the product was purified by washing several times with ethanol and drying overnight under vacuum. The obtained AgSF powder was insoluble in common organic solvents, but could be well dispersed in 1,1,2-trichlorotrifluoroethane (F113). The AgSF was drop-coated using F113 on a polystyrene coated silicon wafer. Polystyrene was used as a polymer glue to increase the adhesion between the AgSF film and silicon substrate. A clean silicon wafer was prepared by piranha solution washing,

and polystyrene (1 wt%, $CHCl_3$ solution) was spin-coated using a Laurell model WS-400A-6NPP/LITE spin-coater at 3000 rpm for 30 s.

Antifouling and antibacterial test

PAO1 was used as a model microorganism to test the antifouling and antibacterial properties. This strain can be observed under a fluorescent microscope due to the presence of the green fluorescent protein. The bacterial suspension was prepared as described in previous study [49]. Sample-coated silicon wafers were soaked in 2 mL of a bacterial suspension in a 24-well culture dish for 9 h at 50 rpm, 25 ^{o}C. The initial population of PAO1 was adjusted to 1 x 10^8 CFU/mL by measuring the optical density at 600 nm. After soaking for 9 h, the bacteria adhered to sample surface was observed through a confocal laser scanning microscopy (Eclipse 90i, Nikon, Japan), and the surface coverage was measured by the image processing software (i-solution, IMT technologies, USA). To examine the viability of bacteria, a viability test was carried out using the Live/Dead *Baclight* bacterial viability test kit (Molecular Probes, Carlsbad, CA). The living bacteria appeared green when observed under a fluorescent microscope with a fluorescent isothiocyanate filter, whereas the inactivated (or dead) bacteria appeared red with a tetramethylrhodamine isothiocyanate filter. Five microscopy images were captured per sample, and the average number and standard deviation of covered bacterial were calculated.

Characterization

The elemental composition of AgSF was evaluated by X-ray photoelectron spectroscopy (XPS, SIGMA PROBE) from ThermoVG (UK). X-ray diffraction was carried out using a Bruker D8 (DISCOVER, Germany). The infrared (IR) spectra were recorded in the attenuated total reflectance (ATR) mode over the frequency range, 4000-650 cm^{-1}, on a Nicolet 6700 instrument (Thermo Scientific, USA). Thermogravimetric analysis (TGA) was carried out on a TA instrument TGA-2050 at a heating rate of 10 ^{o}C/min. Sonication was performed using a Branson 3510 (Branson Ultrasonic Corporation, Danbury, CT). Field emission scanning electron microscopy (FE-SEM) images were obtained using a JSM-6700F and SUPRA 55VP. Contact angle images were obtained using a Krüss DSA10 contact angle analyzer interfaced to drop shape analysis software. These contact angles were measured more than four times on independently prepared films and the average values were used.

3.3. Results and Discussions.

The AgSF was prepared by mixing a $AgNO_3$ with excess PFDT and TEA in ethanol. After stirring for 24 h, the AgSF was obtained as a white solid precipitate from the following equation.

$$AgNO_3 + HS(CH_2)_2(CF_2)_8F \rightarrow AgS(CH_2)_2(CF_2)_8F + HNO_3 \qquad (3.1)$$

Others also prepared silver thiolate compounds by mixing silver salts with alkanethiols and the products had a silver to thiolate molar ratio of 1:1, as shown in equation (3.1) [22,25,28]. AgSF having various shapes (irregular, plate, rod, and wire) were prepared by varying the molar ratio of $AgNO_3$/PFDT in the reactions. The basic compound, TEA, was added as an acid receptor. When the AgSF was prepared without TEA, no specific shapes (wire or plate) were obtained, and powders were obtained instead (Figure. 3.2a). Therefore, acid (HNO_3) prevents the formation of the shapes of the products possibly by weakening the molecular interaction of the AgSF on the molecular level. TEA can be used as an acid receptor and/or reaction promoter to help the reactions [34-37]. Although the other basic compounds such as hexylamine (Figure. 3.2b) and 1,8-diazabicyclo-7-undecene (Figure. 3.2c) can act as a basic compound to produce AgSF having some shapes, TEA (Figure. 3.2d) was chosen as the acid receptor in the synthesis of AgSF because the shape control was more facile. Elemental analysis and ATR-IR showed that no amine compounds from TEA remained in the AgSF. Therefore, TEA assists in the shape formation and can be removed easily through a purification process.

Figure. 3.3 shows FE-SEM images of the AgSF synthesized from different $AgNO_3$/PFDT molar ratios. AgSF having irregular shape was produced when the $AgNO_3$/PFDT molar ratio was 1/1 (Figure. 3.3a). AgSF with plate shape was obtained when larger amounts of $AgNO_3$ ($AgNO_3$/PFDT = 10/1 or 2/1) were used, as shown in Figure. 3.3b and 3.3c. On the other hand, AgSF with wire shape was produced when larger amounts of PFDT ($AgNO_3$/PFDT = 1/2 and 1/10) was used, as shown in Figure. 3.3d and 3.3e. Changing the $AgNO_3$/PFDT molar ratio from 2/1 to 10/1 or from 1/2 to 1/10 did not affect the size or shape of the AgSF. A reaction with $AgNO_3$/PFDT = 1/1 did not produce wires, indicating that the smallest amount of PFDT to form the wires is between 1/1 - 1/2 in the molar ratio of $AgNO_3$/PFDT. Such plates or wires were not produced when alkanethiols such as decanethiol or dodecanethiol was used instead of PFDT using the same reaction [19,21,25]. Therefore the formation the wire structures should be highly related with the strong hydrophobic interactions between the perfluoroalkyl groups in PFDT.

Although AgSF having wire shape is insoluble in common organic solvents, it could be dispersed in F113. Therefore, films could be prepared using a dispersed solution of AgSF having wire shape in F113 to analyze the surface property and other characterization. On the other hand, AgSF having a plate or irregular shape was insoluble and not dispersible in any solvent, and a further study could not be performed. Elemental analysis results shown in the next paragraph indicate that the AgSF having wire shape and other shape have the same chemical composition. Therefore the different solubility behavior of the

AgSF having different shapes should be related to the ordered layer structures on the molecular level. The AgSF having wire shape showed micro-/nano-sized hierarchical structures. Highly fluorinated materials having hierarchical structure have a high probability of exhibiting superhydrophobic properties as reported by others [4-6]. When AgSF having wire shape was treated by sonication, the wires were broken to form rod shapes. For example, rod shape AgSF with 3 - 20 aspect ratios was produced when they were irradiated with ultrasound for 2 h, as shown in Figure. 3.3f. When the ultrasound was irradiated for longer than 3 h, the rod shapes broke down into irregular shapes.

A silver-thiolate complex is composed of one thiolate group per silver atom [19-26]. Elemental analysis also indicated that AgSF having a wire shape has a one to one composition. The theoretical value of carbon for AgSF having a one to one composition is 20.44 wt %. Elemental analysis revealed a carbon content of 21.13 wt %. TGA also showed that the amount of residual AgSF was identical to the silver content obtained by theoretical calculations within experimental error. The same elemental analysis and TGA results were observed from AgSF having irregular shape prepared by a reaction with $AgNO_3$/PFDT = 1/1. This suggests that the AgSF prepared at different molar ratios have an identical chemical composition, even though their shapes are different.

A supramolecular assembly of a silver-alkanethiolate complex has highly ordered layered structures [19,20,25,29]. The wire shape AgSF was also found to have an ordered structure from the X-ray study. A series of ordered reflections indicating a layered structure were observed. The formation of the wire structure of AgSF is believed to

depend on the reaction conditions at the beginning of the reaction because the products are formed as a precipitate immediately when the reactants are mixed. Since the wire shapes are formed when larger amounts of PFDT are used, definitely hydrophobic condition should assist in the formation of a wire shape structure. Similarly, others also reported the formation of a wire shape structure from the silver complexes under similar conditions. Yonezawa *et al.* reported the formation of long fibrous aggregates of silver nanoparticles stabilized by PFDT, where the integrated structure of PFDT molecules on the fibrous aggregation gives the wire structures [29,30]. Möller *et al.* presented silver nanocables consisting of a silver core and an oleic acid organic shell with a long alkyl chain [38]. Similarly, in the present case, hydrophobic PFDT chains having layered structures on the molecular level grow to a wire shape complex as other fatty acid and long carboxylate molecules forms the wire shapes with the silver nanostructures.

Since the AgSF contains silver ions and perfluoroalkyl chains, it can be used for various coating and biomedical applications. Silver ions can be used for the formation of silver nanoparticles, which have excellent antibacterial properties [21,25,38-40] and the perfluoroalkyl group can impart a very low surface energy [10,41-43]. Among the valuable properties, the superhydrophobic, antifouling and antibacterial properties were studied.

An attempt was made to prepare silver nanoparticles from AgSF by UV irradiation. Thin AgSF films were prepared by drop-coating on a polystyrene-coated silicon wafer. Silver nanoparticles were generated on the wires when the AgSF films (Figure. 3.4a)

were irradiated with UV light. Small silver nanoparticles with a diameter less than 20 nm were obtained after UV irradiation for 1 day. The size of the silver nanoparticles increased with the irradiation time, and finally became approximately 50 ~ 100 nm after 7 days (Figure. 3.4b). XRD and XPS showed that the silver atoms in the UV-treated AgSF were in the Ag0 state. XRD peaks of UV-treated AgSF at 38.2^{o} and 44.4^{o} can be assigned to the (111) and (200) crystalline planes of the face-centered cubic (fcc) phase of silver (JCPDS File No. 01-089-3722). The Ag $3d_{3/2}$ and Ag $3d_{5/2}$ XPS peaks of AgSF were observed at 368.2 and 374.1 eV (as referenced to the 285 eV C 1s peak). After UV-irradiation, these peaks were down-shifted to 367.8 and 373.8 eV, respectively. These peak positions were the same as those observed from the zero valent silver reported in the literature (367.9 ± 0.1, 373.9 ± 0.1) and the difference in the two peaks observed was precisely the same as the difference (6 eV) reported in the literature [44,45]. As a result, silver nanoparticle-coated AgSF wires (UV-treated AgSF) were prepared simply by UV irradiation.

The surface properties of the AgSF films prepared on polystyrene-coated silicon wafers were evaluated by measuring the water contact angle. Very large water contact angles (> 150^{o}) were observed on the AgSF surface, as shown in Figure. 3.4c. Images of the water droplet were only possible after slight contact with the AgSF surface. Otherwise, the drops runoff from the surface or remain attached to the tip of the needle used to put them on the surface for contact angle measurements (very low sliding angle). The water droplets became very unstable on this surface, and gentle vibrations could make the water

droplets roll away. Therefore, the AgSF films have superhydrophobic properties [4-11]. The hydrophobicity is affected by both the surface tension and surface roughness. The superhydrophobicity of AgSF is due to a combination of a hierarchical micro-/nano-sized wire shape structure and the low surface energy property of the fluorine component. The superhydrophobic property remained for more than 6 months under atmosphere conditions. After UV irradiation, the AgSF surface loses the superhydrophobic property and shows smaller water contact angles ($110^{o} \pm 2$, Figure. 3.4d). The silver nanoparticles formed by UV irradiation reduce the water contact angle because silver component have higher surface energy than that of fluorinated materials [46]. Therefore, an AgSF surface containing silver nanoparticles on the surface has a smaller water contact angle than a pure AgSF surface having a wire shape.

The antifouling properties of AgSF and UV-treated AgSF surface was determined by calculating the surface coverage after soaking in the bacterial suspension for 9 h. Polystyrene was used as a reference for comparison. As shown in Figure. 3.4e, the surface coverage on AgSF was much less than that on polystyrene; the surface coverage of PAO1 on AgSF was less than 1 %, whereas the coverage on the polystyrene surface was approximately 18 %. Many efforts have been made to examine the mechanism for the antifouling property [41-43,47,48], but there are only a few reports on the relationship between superhydrophobic surfaces and antifouling properties [10,11]. Bacterial adhesion on the surfaces is affected by their physicochemical properties, such as chemical composition, roughness, surface energy, surface charge, and mechanical strength

[10,11,41]. The antifouling property of AgSF can be due to the superhydrophobicity of this surface because the superhydrophobic surfaces decrease the contact area between the solid surface and surrounding solution, water, thereby minimizing the chances of bacterial reaching the surface [10]. After UV irradiation, the surface lost its superhydrophobic property (water contact angle = 110^{o}), and the surface coverage of bacteria increased (approximately 9 %, Figure. 3.4f), which agrees with the above suggestion quite well. Still the bacterial coverage on this surface was less than that on the polystyrene.

To measure the antibacterial properties of AgSF, a viability test was carried out using the Live/Dead Baclight bacterial viability test kit. Figure. 3.4e and 3.4f show an image of PAO1 cells that remain on the AgSF and UV-treated AgSF surface, respectively. Living bacteria appear green, whereas the inactivated (or dead) bacteria appear red. Figure. 3.5 shows the bacterial surface coverage and bacterial inactivation on the polystyrene, AgSF, and UV-treated AgSF surfaces. The polystyrene surface did not show antibacterial properties and all the adhered bacteria showed a green color. On the other hand, both AgSF and UV-treated AgSF showed antibacterial properties; AgSF shows antibacterial properties about 77 % of bacterial inactivation value and almost 100 % of bacteria are killed on UV-treated AgSF. Since AgSF having wire shape can be used as a precursor material to synthesize silver nanomaterials, other AgSF having different shapes, such as powders, plates, and rods can be also used as precursor materials for the preparation of hybrid metallic silver nanomaterials with a variety of structure shapes. Additionally, they can also be used as additives to produce surfaces having antifouling and/or antibacterial

properties. In addition to the above preliminary results, the applications of these materials have largely been unexplored.

3.4. Conclusions

A superhydrophobic silver-perfluorodecanethiolate complex having antifouling and antibacterial properties was demonstrated. The AgSF was prepared simply by mixing silver nitrate and perfluorodecanethiol, and fluorinated micro-/nano-sized hierarchical structures were formed during the reaction. AgSF films on polystyrene-coated silicon wafers exhibited superhydrophobic properties as well as excellent antifouling properties against Pseudomonas aeruginosa PAO1 bacteria. Furthermore, silver nanoparticles could be formed on the AgSF film by UV irradiation and show excellent antibacterial properties. We believe that AgSF is a good candidate for a range of applications because it can have superhydrophobic, antifouling, and antibacterial properties.

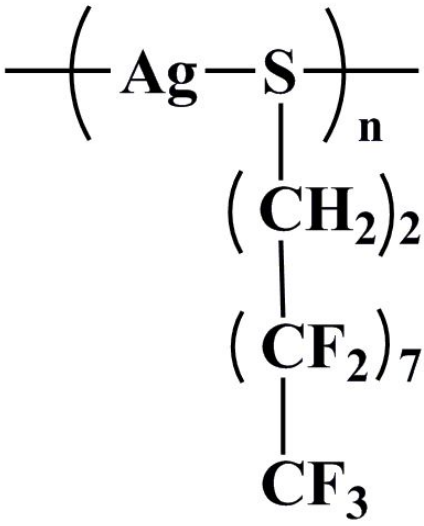

Figure. 3.1. Silver-perfluorodecanethiolate complex (AgSF).

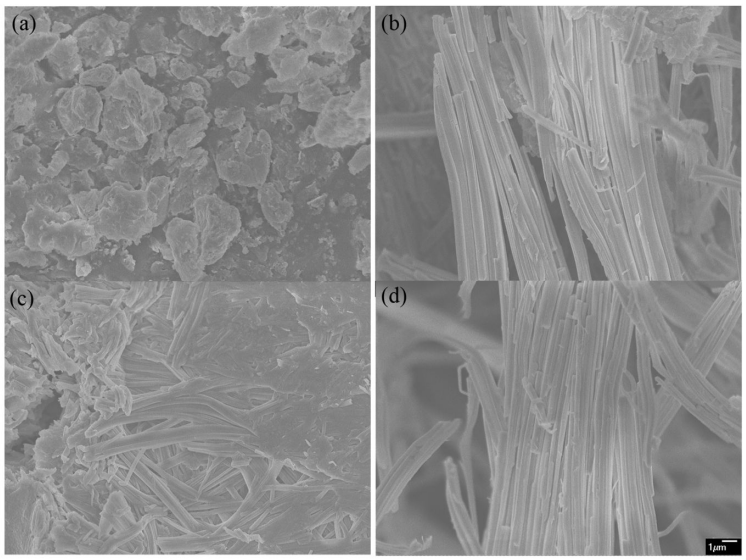

Figure. 3.2. FE-SEM images of AgSF prepared with/without basic compound, where (a) without basic compound, with (b) hexylamine, (c) 1,8-diazabicyclo-7-undecene, (d) triethylamine.

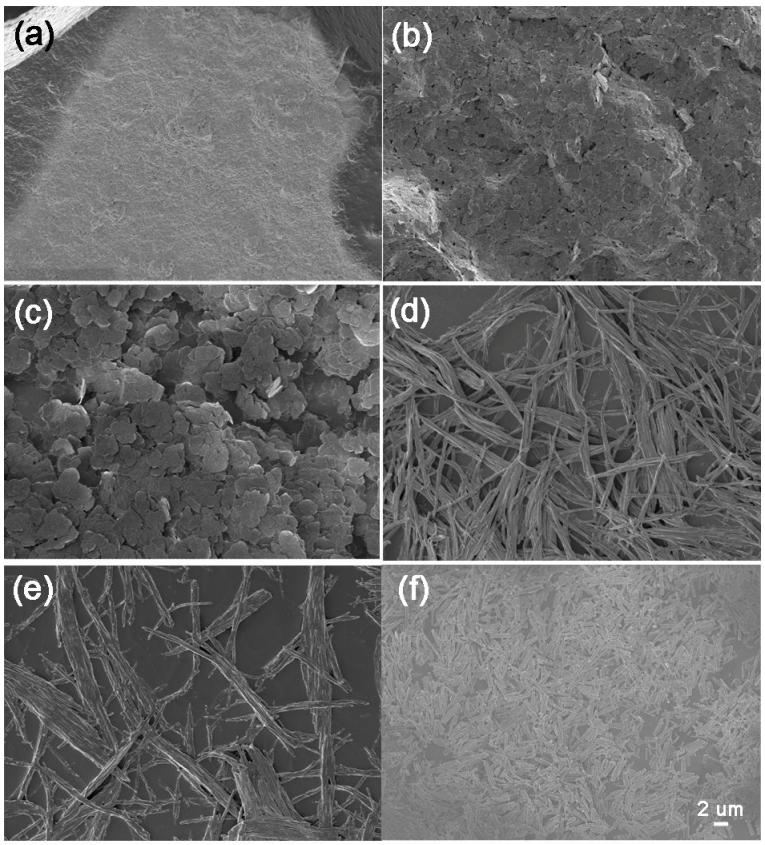

Figure. 3.3. FE-SEM images of AgSF synthesized from different molar ratio of silver nitrate/PFDT = (a) 1/1, (b) 10/1, (c) 2/1, (d) 1/2, (e) 1/10. (f) FE-SEM images of AgSF (1/2) after sonication for 2 h.

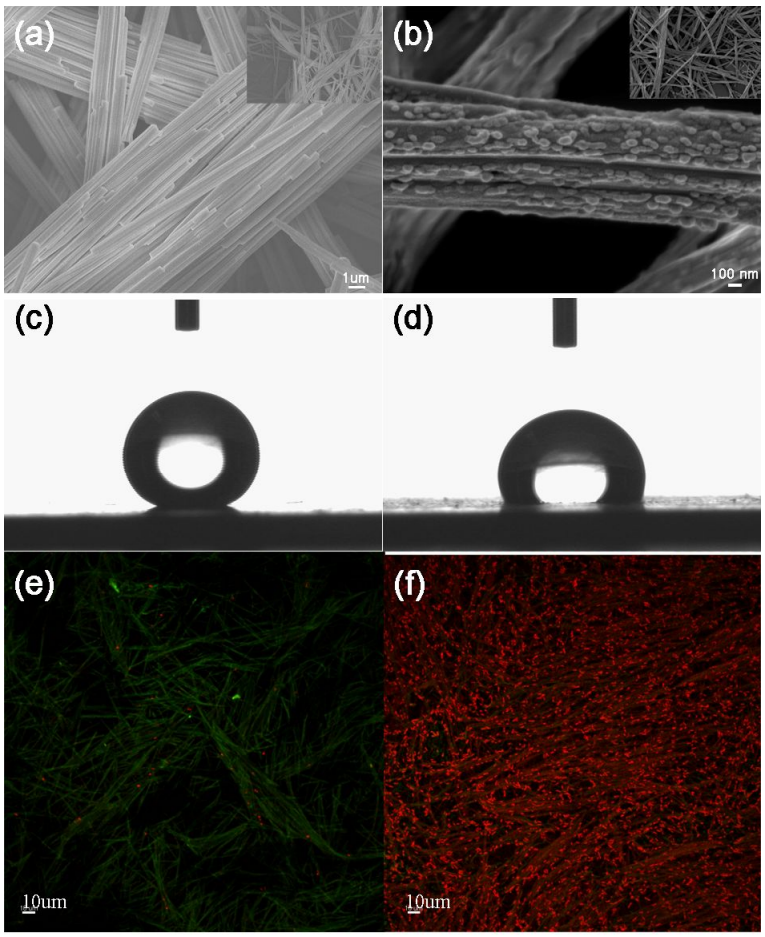

Figure. 3.4. FE-SEM images of the (a) AgSF and (b) UV-treated AgSF. Contact angle images of water on (c) AgSF and (d) UV-treated AgSF surface. Live/dead staining images of PAO1 cells that remain on the (e) AgSF and (f) UV-treated AgSF surface after bacterial adhesion test for 9 h (green color - live; red color - inactivated or dead).

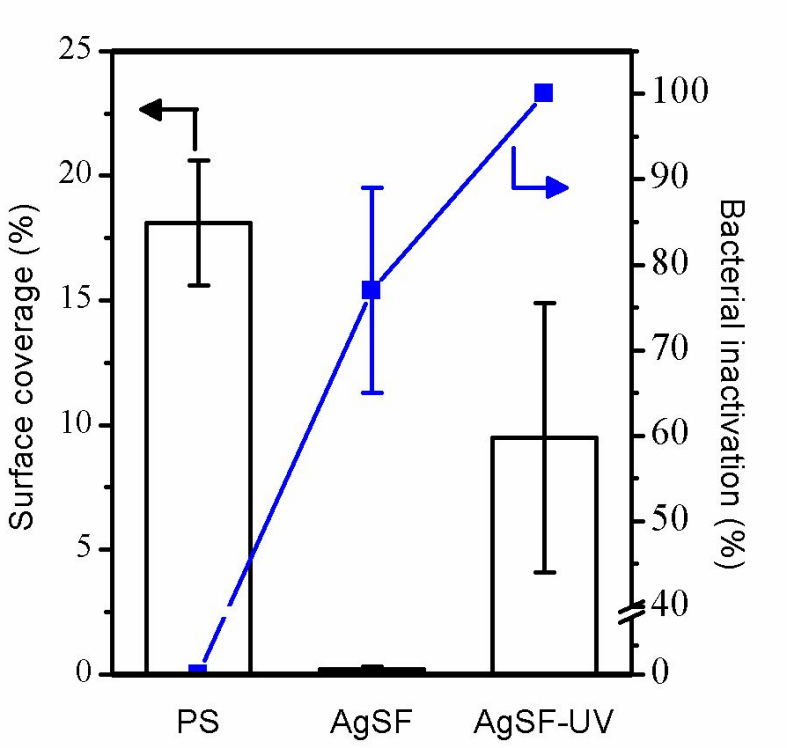

Figure. 3.5. Surface coverage and bacterial inactivation on the polystyrene, AgSF, and UV-treated AgSF surfaces.

3.5. References

[1] Turri, S.; Scicchitano, M.; Marchetti, R.; Sanguineti, A.; Radice, S., In *Fluoropolymers, Vol. 2* (Eds: G. Hougham, P. E. Cassidy, K. Johns, T. Davidson), Plenum Press, New York 1999.

[2] Tsibouklis, J.; Nevell, T. G. *Adv. Mater.* **2003**, *15*, 647.

[3] Chung, J.-S.; Kim, B. G.; Sohn, E.-H.; Lee, J.-C. *Macromolecules* **2010**, *43*, 10481.

[4] Zhang, J. L.; Li, J. A.; Han, Y. C. *Macromol. Rapid Commun.* **2004**, *25*, 1105.

[5] Singh, A.; Steely, L.; Allcock, H. R. *Langmuir* **2005**, *21*, 11604.

[6] Mabry, J. M.; Vij, A.; Iacono, S. T.; Viers, B. D. *Angew. Chem. Int. Ed.* **2008**, *47*, 4137.

[7] Feng, L.; Li, S.; Li, Y.; Li, H.; Zhang, L.; Zhai, J.; Song, Y.; Liu, B.; Jiang, L.; Zhu, D. *Adv. Mater.* **2002**, *14*, 1857.

[8] Zhang, X.; Shi, F.; Niu, J.; Jiang, Y.; Wang, Z. *J. Mater. Chem.* **2008**, *18*, 621.

[9] Ma, M.; Hill, R. M. Curr. Opin. Colloid Interface Sci. **2006**, 11, 193.

[10] Genzer, J.; Efimenko, K. *Biofouling* **2006**, *22*, 339.

[11] Marmur, A. *Biofouling* **2006**, *22*, 107.

[12] Furstner, R.; Barthlott, W.; Neinhuis, C.; Walzel, P. *Langmuir* **2005**, *21*, 956.

[13] Sun, T.; Tan, H.; Han, D.; Fu, Q.; Jiang, L. *Small* **2005**, *1*, 959.

[14] Sun, T.; Qing, G.; Su, B.; Jiang, L. *Chem. Soc. Rev.* **2011**, *40*, 2909.

[15] Zhang, X.; Shi, F.; Yu, X.; Liu, H.; Fu, Y.; Wang, Z.; Jiang, L.; Li, X. *J. Am. Chem.*

Soc. **2004**, *126*, 3064.

[16] Shirtcliffe, N. J.; McHale, G.; Newton, M. I.; Chabrol, G.; Perry, C. C. *Adv. Mater.* **2004**, *16*, 1929.

[17] Lu, X.; Zhou, J.; Zhou, Y.; Qiu, Y.; Li, J. *Chem. Mater.* **2008**, *20*, 3420.

[18] Sun, T.; Feng, L.; Gao, X.; Jiang, L. *Acc. Chem. Res.* **2005**, *38*, 644.

[19] Bensebaa, F.; Ellis, T. H.; Kruus, E.; Voicu, R.; Zhou, Y. *Langmuir* **1998**, *14*, 6579.

[20] Parikh, A. N.; Gillmor, S. D.; Beers, J. D.; Beardmore, K. M.; Cutts, R. W.; Swanson, B. I. *J. Phys. Chem. B* **1999**, *103*, 2850.

[21] Hu, L.; Zhang, Z.; Zhang, M.; Efremov, M. Y.; Olson, E. A.; de la Rama, L. P.; Kummamuru, R. K.; Allen, L. H. *Langmuir* **2009**, *25*, 9585.

[22] Cha, S.-H.; Kim, J.-U.; Kim, K.-H.; Lee, J.-C. *Chem. Mater.* **2007**, *19*, 6297.

[23] Zhang, Y. X.; Zeng, H. C. *Adv. Mater.* **2009**, *21*, 1.

[24] Kim, J.-U.; Cha, S.-H. Shin, K.; Jho, J. Y.; Lee, J.-C. *J. Am. Chem. Soc.* **2005**, *127*, 9962.

[25] Kim, S.-E.; Han, Y.-H.; Lee, B. C.; Lee, J.-C. *Nanotechnology* **2010**, *21*, 075302.

[26] Cha, S.-H.; Kim, K.-H.; Lee, W.-K.; Lee, J.-C. *J. Ind. Eng. Chem.* **2010**, *16*, 816.

[27] Chen, S.; Hu, C.; Chen, L.; Xu, N. *Chem. Commun.* **2007**, 1919.

[28] Xu, X.; Zhang, Z.; Yang, J.; Colloids Surf. A: Physicochem. Eng. Asp. **2010**, 355, 163.

[29] Yonezawa, T.; Onoue, S.; Kimizuka, N. *Adv. Mater.* **2001**, *13*, 140.

[30] Yonezawa, T.; Onoue, S.; Kimizuka, N. *Langmuir* **2001**, *17*, 2291.

[31] Dass, A.; Guo, R.; Tracy, J. B.; Balasubramanian, R.; Douglas, A. D.; Murray, R. W. *Langmuir* **2008**, *24*, 310.

[32] Im, J.; Chandekar, A.; Whitten, J. E. *Langmuir* **2009**, *25*, 4288.

[33] Gentilini, C.; Evangelista, F.; Rudolf, P.; Franchi, P.; Lucarini, M.; Pasquato, L. *J. Am. Chem. Soc.* **2008**, *130*, 15678.

[34] Lendlein, A.; Jiang, H.; Jünger, O.; Langer, R. *Nature* **2005**, *434*, 879.

[35] DeRosa, M. C.; Hodgson, D. J.; Enright, G. D.; Dawson, B.; Evans, C. E. B.; Crutchley, R. J. *J. Am. Chem. Soc.* **2004**, *126*, 7619.

[36] Hsu, S. L.-C.; Wu, R.-T. *Mater. Lett.* **2007**, *61*, 3719.

[37] Wu, R.-T.; Hsu, S. L.-C. *Mater. Res. Bull.* **2008**, *43*, 1276.

[38] Weichold, O.; Hsu, S.-C.; Möller, M. *J. Mater. Chem.* **2006**, *16*, 4475.

[39] Kim, J. S. *J. Ind. Eng. Chem.* **2007**, *13*, 718.

[40] Youn, M. H.; Lim, Y. M.; Gwon, H. J.; Park, J. S.; An, S. J.; Nho, Y. C. *Macromol. Res.* **2009**, *17*, 813.

[41] Krishnan, S.; Weinman, C. J.; Ober, C. K. *J. Mater. Chem,* **2008**, *18*, 3405.

[42] Krishnan, S.; Wang, N.; Ober, C. K.; Finlay, J. A.; Callow, M. E.; Callow, J. A.; Hexemer, A.; Sohn, K. E.; Kramer, E. J.; Fischer, D. A. *Biomacromolecules* **2006**, *7*, 1449.

[43] Finlay, J. A.; Krishnan, S.; Callow, M. E.; Callow, J. A.; Dong, R.; Asgill, N.; Wong, K.; Kramer, E. J.; Ober, C. K. *Langmuir* **2008**, *24*, 503.

[44] Kang, S. Y.; Kim, K. *Langmuir* **1998**, *14*, 226.

[45] Wagner, C. D.; Riggs, W. M.; Davis, C. E.; Mouler, J. F., *In Handbook of X-ray Photoelectron Spectroscopy* (Eds: G. E. Muilenberg), Eden Praire, MN, Perkin-Elmer Corporation 1979 p 122.

[46] Osman, M. A.; Keller, B. A. *Appl. Surf. Sci.* **1996**, *99*, 261.

[47] Jr. Brady, R. F.; Singer, I. L. *Biofouling* **2000**, *15*, 73.

[48] Ye, S.; Mahumdar, P.; Chisholm, B.; Stafslien, S.; Chen, Z. *Langmuir* **2010**, *26*, 16455.

[49] Shim, S.; Hong, S. H.; Tak, Y.; Yoon, J. *Biofouling* **2011**, *27*, 217.

Chapter 4

Healable Polymethacrylate Films Having Photocrosslinkable Cinnamoyl Side Group

4.1. Introduction

Healing is a very natural phenomenon on living things and many efforts have been made to realize healing properties using artificial materials. Healable materials offer enormous possibilities, particularly for applications in which long-term reliability in poorly accessible areas is important. Additionally, healable material would be ideal for applications that are prone to damage, such as surface coatings.[1-4] During the past 10 years, healable materials have received much interest, and many researchers have demonstrated smart materials having healing properties.[5-14] These materials can achieve healing either intrinsically via reversible bonds presents in the material itself or extrinsically via a pre-added healing agent in response to some external stimulus. Reversible reaction such as Diels-Alder [7-9] and cycloaddition [10,11] have been used to recover the original properties of materials, because these reversible reations show different phases that can increase mobility of the material components. In contrast, pre-added healing agents such as liquid monomers, generally stored in microcapsules or in a vascular system, are released when a crack is generated.[12-14] Then, the released liquid healing agents polymerizes in the crack plane with the help of a catalyst and their phase is changed from a mobilable liquid to hard matrix, which results in rebinding of the crack faces with good mechanical properties.

A prerequisite for healing cracked material is generating a mobile phase, that can close the cracks. In general, mobile phases are generated with small molecules such as debonded moieties, liquid healing agents (monomers) and hydrogelsn and then restore the

cracked morphology to a pristine state.[4] During the healing process, these mobile phase materials should be immobilized to fully restore the mechanical properties, because the materials require not only the liquidity of the cracked area for healing but also require hardness for use in a variety of application fields. These two distinct requirements are generally contrary to each other and not easy to obtain. It is evident that a polymer system is the best candidate that achieves both mobility for healing and hardness to resist the crack due to their ability to reach different states and their special molecular architectures. Several studies have been published on healable polymers and many fresh strategies and approaches to develop healing properties have been investigated.[15-20] However, only a few studies have reported on the influence of glass transition temperature (T_g) and polymer structure on healing properties, even though these factors are major parameters to determine polymer properties. Wool *et al.* reported craze healing in atatic polystyrene glasses and provided a microscopic theory for healing of polymer and polymer/polymer interfaces.[21-23] Boiko *et al.* also reported healing of a polymer/polymer interface in the vicinity of the T_g.[24-26]

Based on these considerations, we synthesized cinnamoyl functionalized polymethacrylate derivatives having healing and photo-responsive hardening properties. A series of polymethacrylates having different T_g values were systematically studied. Studies on the relationship between healing properties and T_g are helpful for other investigations about healing, and they provide a practical basis for the healing mechanism via thermal treatments. Furthermore, T_g controlled polymethacrylate derivatives

containing cinnamoyl side group showed good healing properties at 80 ^{o}C, and the mechanical properties could be controlled by UV irradiation at an appropriate wavelength.

4.2. Experimental

Materials

Ethyl methacrylate, butyl methacrylate, hexyl methacrylate, poly(2-hydroxyethyl methacrylate) (PHEMA), cinnamoyl chloride, hydrocinnamoyl chloride and pyridine were purchased from Sigma-Aldrich Chemical Co. Azobisisobutyronitrile (AIBN) was purchased from TCI. All reagents and solvents were used without further purification.

Synthesis

Preparation of poly(*n*-alkyl methacrylate)s

Poly(ethyl methacrylate) (PEMA), poly(butyl methacrylate) (PBMA) and poly(hexyl methacrylate) (PHMA) were prepared by conventional free radical polymerization from ethyl methacrylate, butyl methacrylate and hexyl methacrylate, respectively. Toluene (50 wt%) was used as the polymerization solvent, and AIBN (1 wt%) was used as the initiator. The reaction mixture was stirred at 60 ^{o}C for 24 h and then poured into methanol. The precipitate was further purified by several precipitations from a tetrahydrofuran (THF) solution into methanol and then dried under vacuum at room temperature. The products were obtained at > 80 % yield after purification. The weight average molecular weight (M_w) and polydispersity index of the polymers were 120,800 and 2.42 for PEMA, 60,600 and 2.16 for PBMA, and 135,800 and 2.25 for PHMA, respectively.

Preparation of poly(2-cinnamoyloxyethyl methacrylate) (PCEMA)

Cinnamoyl chloride (3 g, 18 mmol) was added to a stirred solution of PHEMA (2 g, 15.2 mmol) in 100 mL of pyridine under a nitrogen atmosphere. The reaction mixture was stirred at room temperature for 24 h and then poured in water. The precipitate was further purified by several precipitations from a THF solution into hexane, and then dried under vacuum at room temperature. The product was obtained at a > 90 % yield after the purification steps. The M_w and polydispersity index of the polymer were 62,100 and 1.93, respectively. ^{1}H nuclear magnetic resonance (NMR) spectra of PCEMA ($CDCl_3$, δ in ppm): 1.06 (m, 3H), 1.83 (m, 2H), 4.09 (m, 2H), 4.21 (m, 2H), 6.47 (m, 1H), 7.32 (m, 3H), 7.51 (m, 2H), and 7.61 (m, 1H).

Preparation of random copolymers of PHEMA and PCEMA (PCEMA-#s)

A series of PCEMA-#s (where # is the mol % of monomeric units containing cinnamoyl side group, 10, 30, 50 and 70) having different cinnamoyl side group contents was synthesized to observe the effect of T_g on healing properties. These polymers were prepared using the identical reaction procedure as PCEMA except for the predetermined amount of cinnamoyl chloride. We calculated the degree of substitution using the ^{1}H NMR results by comparing the multiplet at 1.06 (3H) from the backbone and the multiplet at 6.47 (1H) from the cinnamoyl double bond.

Preparation of poly(2-hydrocinnamoyloxyethyl methacrylate) (PCEMA-H)

PCEMA-H having a hydrocinnamoyl side group was synthesized to observe the effect

of a double bond in the cinnamoyl side group. This polymer was prepared as the identical reaction procedure with PCEMA except that hydrocinnamoyl chloride was used instead of cinnamoyl chloride.

Film preparation

Polymer films (20 ~ 100 μm thick) were prepared by casting a 20 wt% solution of the samples in *N*-methyl-2-pyrrolidone onto a glass substrate. The films were then dried for 6 h at 40 ^{o}C and 12 h at 60 ^{o}C to remove residual solvent. Photocrosslinking was performed using a 4 W 365 nm UV lamp and photocleavage was performed using a 4 W 254 nm UV lamp (Spectronics Corp., Westbury, NY, USA). In either case, the lamp was placed above the sample at a distance of 3 cm.

Analysis

^{1}H NMR spectra (500 MHz) were measured in $CDCl_3$ using a Bruker Avance 500 instrument. The M_w and polydispersity index were obtained by gel permeation chromatography (GPC, Viscotek) using a diffractometer as the detector. THF was used as the solvent, and monodispersed polystyrene was used as the standards. Differential scanning calorimetry (DSC, TA Instruments 2920 differential scanning calorimeter) was carried out at heating and cooling rates of 5 ^{o}C min^{-1}. To eliminate the effect of thermal history on the sample transitions, all samples were heated to 200 ^{o}C and held at that temperature for 5 min before cooling. The transition temperatures and enthalpy changes

were obtained from the second heating scan. Infrared (IR) spectra were recorded in the attenuated total reflectance (ATR) mode over the frequency range 4000-650 cm^{-1}, on a Nicolet 6700 instrument (Thermo Scientific, USA). Optical microscopy (OM) images were obtained with an optical microscope (ECLIPSE E600 POL, NIKON) equipped with a digital camera (COOLPIX E500, NIKON). Pencil scratch hardness was evaluated with Staedtler pencils (Mars Lumograph, Germany) with different hardnesses.[27,28]

4.3. Results and Discussions.

Healable polymers have attracted attention from many research groups trying to develop effective approaches.[15-20] Among them, the healing process induced by thermal treatment is widely established and reported typically as a Diels-Alder reaction.[7-9,19,20] However, few reports have considered detailed studies on the healing property of polymer films with different T_g. We attempted to model-glass transition contributions to the healing property in a series of poly(*n*-alkyl methacrylate)s. Poly(*n*-alkyl methacrylate)s (n = 2 [PEMA], 4 [PBMA], 6 [PHMA]) were synthesized by conventional free radical polymerization and we obtained identical T_g values as reported previously.[29] The T_g values of PEMA, PBMA and PHMA were 70, 25 and - 20 ^{o}C, respectively. The healing properties of the polymethacrylate series should be influenced by T_g because these polymers have similar chemical structures and do not have any healable moieties such as maleimide-furan (Diels-Alder reaction) or a cinnamoyl group (photocrosslinking reaction) in the polymer structure. The only difference is the side chain length, which affects chain mobility in the polymer film.

The polymer solution was cast on a glass substrate, and a micro-sized artificial scratch (width: 20 ~ 40 μm) was made on the film surface using a razor blade to observe the healing properties of polymer films at various temperatures. Subsequently, thermal treatment was added using a hot plate at different temperatures of 30 ~ 120 ^{o}C for 24 h. Figure 4.2 shows the optical microscopy (OM) images of PEMA (Figure 4.2a-2b) and

PBMA (Figure 4.2c-2d) films treated at 50 (Figure 4.2a and 2c) and 80 ^{o}C (Figure 4.2b and 2d). The healing properties could not be obtained quantitatively but could be qualitatively observed using OM. The left part of Figure 4.2 illustrates the damaged film before heating, whereas the right part illustrates the healed films. When the damaged film was heated to temperatures that were higher than T_g, the damaged area vanished (right part of Figure 4.2b, 2c and 2d). In the case of PHMA, the damage on the polymer film was healed at 20 ^{o}C. Due to the low healing temperature and short healing time, we could not optain a comparison figure of PHMA. The gaps between the T_g and healing temperature were different in each cases. For example, PEMA (T_g = 70 ^{o}C) required an 80 ^{o}C healing temperature to heal the damaged area, whereas PBMA (T_g = 25 ^{o}C) required 50 ^{o}C to healed, which still did not heal the area perfectly. When the PBMA film was treated by heating at 60 ^{o}C, the damaged area vanished completely. PHMA (T_g = - 20 ^{o}C) did not require heating because the room temperature was 40 ^{o}C higher than its T_g. The difference in healing temperatures probably was the result of the diffusion rate of the polymer chain segments. When sufficient heat was applied, the polymer chains crossed the interface of the crack, penetrated the other side, and formed entanglements with chains on the other side without any chemical reactions. Wool and colleagues described the motion of the chain at the polymer/polymer interface based on the reptation model, which was developed by de Gennes.[21,30] They presented a theory for the stages of wetting, diffusion, and randomization at the polymer/polymer interface. When the healing process is conducted on compatible amorphous polymer interfaces above T_g, translational

motions of the segments across the polymer interface occurs and rapid local elastic deformations at the points of contact occur, which is described as wetting. As soon as wetting is established, interdiffusion of segments and randomization follow. Still, a complex and as yet unknown relationship exists between the degree of wetting and diffusion and directly measurable quantities such as changes in crack size and healing time. Figure 4.2 shows that the micro-sized damage in the general polymer films was healed by heating at a higher temperature relative to the T_g without any healable moieties and external stimuli such as pressure and/or solvents.

Considering the healing properties of the polymethacrylate series, we designed photocrosslinkable polymethacrylates with low T_g values. The cinnamoyl group was chosen as a photo-responsive moiety. The major drawback of low T_g material is the lack of a mechanical property. The increase in polymer chain mobility for healing and improving the mechanical property are generally contrary to each other. To overcome the weakness of the film surface, photochemical [2+2] cycloaddition of cinnamoyl groups was chosen as a surface hardening reaction, because the cinnamoyl group exhibits a high photosensitivity and particularly efficient photoreversibility. Exposing the cinnamoyl groups to > 300 nm UV irradiation resulted in [2+2] cycloaddition of their double bonds, whereas short exposure to 254 nm led to the photocleavage reaction. Additionally, it has already been reported that the photocrosslinkable cinnamate monomers can be used as a healing agent in a highly crosslinked matrix via UV irradiation.[11] Irradiation with wavelengths longer than 300 nm lead to the crosslinking of adjacent cinnamoyl groups

via formation of a cyclobutane ring, which should increase surface hardness. If the film surfaces are damaged, these crosslinks undergo a photocleavage reaction at 254 nm of irradiation, potentially yielding the original cinnamoyl groups and high chain mobility for healing. Through the reversible photocycloaddition reaction, we tried to obtain a hardness controllable film with a low T_g value. Comparison studies about the effect of heating and/or UV irradiation on the healing property were established.

Poly(2-cinnamoyloxyethyl methacrylate) (PCEMA) was prepared by an one-step modification method under a moderate conditions. The hydroxyl groups of PHEMA were easily reacted with cinnamoyl chloride in a pyridine at room temperature without catalysts or additives. Although the reaction conditions were mild, the degrees of substituted side chains was higher than 99%. The polymer analogous reaction is a useful reaction method to easily obtain high molecular weight polymers with desirable properties.[31-33] In the case of PCEMA, we controlled the T_g easily with photo-responsive cinnamoyl side groups using a polymer analogous reaction. PCEMA-#s where # is 10, 30, 50 and 70 were synthesized and characterized by DSC to investigate the effect of the side chain contents on the T_g of the PHEMA derivatives. Figure 4.3 shows the endothermic traces of PHEMA, PCEMA (100 % cinnamoyl side group content) and PCEMA-#s. All samples were first heated to 200 ^{o}C to remove thermal history, then cooled and heated at a rate of 5 ^{o}C/min. The T_g values of PCEMA and PCEMA-# were observed at 60 ~ 100 ^{o}C and decreased with increasing degree of substitution compared with that of PHEMA indicating that the cinnamoyl side group acts as a plasticizer in the

polymer.[31,34]

The healing properties of PCEMA having different cinnamoyl side group contents were tested with identical experimental procedures as described above for the polymethacrylate series. As anticipated, the damaged PCEMA-#s and PCEMA films were healed when the healing temperatures were 10 ~ 20 ^{o}C higher than their T_g. ATR-IR and OM measurements were used to further examine the chemical reactions and healing properties on the film surface. In contrast, we could not observe the any healing properties when the film was irradiated by UV light. In view of the best performance among the series of PCEMA, only the IR spectra and OM images of the PCEMA are provided here as an example (Figure 4.4 and 4.5).

The IR results of the PCEMA film before (pristine, Figure 4.4a) and after heating (Figure 4.4b) showed no chemical changes indicating that chain diffusion across the interface is a major factor for healing on the film surface. The heating condition was at 80 ^{o}C for 24 h. An initial PCEMA film showed IR absorption bands of cinnamoyl C=O and C=C at 1713 and 1637 cm^{-1}, respectively. Identical absorption spectra were obtained when the films were heated indicating that the cycloaddition reaction or other unexpected reactions did not progressed during the thermal treatment. In contrast, carbonyl absorption shifted to 1734 cm^{-1} upon irradiation of the PCEMA film with UV using a 365 nm lamp, and C=C absorption almost disappeared (Figure 4.4c), which confirmed photocrosslinking of the cinnamoyl side group.[11] This result indicates that the photocrosslinking reaction successfully progressed in the film state. According to a prior

report, the cinnamoyl side groups attached to the polymer backbone undergo two possible chemical reactions: photocycloaddition based on the reversible [2+2] cycloaddition reaction and thermal crosslinking reaction based on the radical reaction which generate the irreversible coordinating bond.[35] The thermal crosslinking reaction occurs when the temperature is high enough to generate the reactive radical on the cinnamoyl group. In the case of PCEMA, only the photocycloaddition reaction progressed due to the relatively low temperature environment of UV irradiation.

Figure 4.5a shows the OM images before and after heating at 80 ^{o}C for 24 h, respectively. Because the T_g of PCEMA was 60.2 ^{o}C lower than the healing temperature, the micro-sized crack vanished completely following thermal treatment. A series of PCEMA-# films showed identical healing properties when treated at suitable healing temperatures (10 ~ 20 ^{o}C higher than each T_g). However, UV irradiation did not lead to healing of damaged PCEMA films (Figure 4.5b, 365 nm UV light for 24 h). The UV irradiated PCEMA film was transparent, insoluble in common organic solvents such as chloroform or THF and harder than the pristine PCEMA film, indicating that the crosslinking based on photocycloaddition was successfully conducted, and that the mechanical properties improved. However, chain mobility decreased during the crosslinking reaction and actual micro-sized scratches did not heal. When the damaged films were heated to 80 ^{o}C during UV irradiation (Figure 4.5c), slightly better healing properties were observed compared with the cases that were only subjected to UV irradiation. The film healed by heating without UV irradiation showed the best healing

properties among the three conditions. Thus, UV irradiation increased the surface hardness while reducing the molecular chain diffusion at the damaged area, which lead to the poor healing property. The photocrosslinking reaction assists the healing process in highly flexible environments such as in a hydrogel or macromonomer system.[11,18,36] If the matrix is not flexible enough (in the case of PCEMA), the crosslinking between cinnamoyl groups could restrict molecular diffusion and decrease healing.

Additionally, poly(2-hydrocinnamoyloxyethyl methacrylate) (PCEMA-H) was prepared and characterized using identical procedures to further understand the influence of the double bond in the cinnamoyl side group during the healing process via healing and/or UV irradiation. The healing properties, as stated above, were mainly affected by the T_g values during thermal treatment. The absence of double bonds in the cinnamoyl group affected side chain ordering, and PCEMA-H had a lower T_g value (24.6 ^{o}C) than that of PCEMA (60.2 ^{o}C). The decrease in T_g slightly affected the healing properties (lower required healing temperature than that for PCEMA) but it is nothing more or less than PBMA, because the PCEMA-H does not contain any photo-responsive functional groups that can induce surface hardening.

Considering the UV irradiation results and the crosslinking of the cinnamoyl side group, the mechanical properties of the PCEMA films increased, whereas the healing properties decreased. This is why the photoreversible reaction should be adapted on a healable polymer. When a crosslinked polymer film is damaged, the decrosslinking reaction, which occurs under 254 nm UV light, makes the films softer, and healing occurs

with heating. After the scratch is healed, the film could gain an initial smooth and hard surface under a crosslinking reaction at 365 nm UV. Figure 4.6 shows the overall strategy of the healing process to obtain the healed hard film, which has similar surface hardness as pristine material. The PCEMA crosslinked film was damaged with a razor blade and subsequently irradiated with a 254 nm UV lamp to decrosslink the hard film for ease of healing. Then, an 80 ^{o}C thermal treatment was conducted. Finally, the healed soft film was irradiated with a 365 nm UV lamp to restore the original hardness of crosslinked the PCEMA film.

The scratch hardness of the film surface was measured by the pencil scratch method at room temperature, and Table 4.1 illustrates the scratch hardness of the polymethacrylates series and PCEMA films treated under different conditions. The scratch hardness values for the poly(*n*-alkyl methacrylate)s were 2H, 3B, and < 7B for PEMA, PBMA, and PHMA, respectively, which corresponded well with their T_g values. The scratch hardness of the initial PCEMA films without any treatment was 2H. When heat were applied at 80 ^{o}C for 24 h, the crack on the film surface was healed, and scratch hardness was still 2H, which agreed with the IR results, indicating than no known reaction occurred with heating. In contrast, when the PCEMA film was cured with 365 nm UV light, the scratch hardness reached 4H, which is hard enough for industrial use.[37] It is interesting that the 254 nm UV light also induced hardening of the film surface and that the scratch hardness increased to 3H when the irradiation time was 24 h.

When initially planning to prepare the PCEMA, we expected that exposing the

crosslinked cinnamoyl groups to 254 nm UV irradiation would result in photocleavage, thus, increasing its chain mobility. However, some reports indicate that 254 nm irradiation not only leads to photocleavage of the crosslinked cinnamoyl groups but also to initiating a crosslinking reaction between cinnamoyl groups via an irreversible process such as a radical reaction different from the photocrosslink reaction products at 365 nm.[38,39] The irradiation time of the 254 nm UV light was an important factor to determine the major reaction between photocrosslinking and photocleavage. In the initial stage, the crosslinked cinnamoyl groups were quickly cleaved into original residues. However, when the irradiation time reached a certain values, the rate of photocrosslink surpassed that of photocleavage. When the initial PCEMA film was irradiated by 254 nm UV light, both photocrosslinking and photocleavage was induced on the PCEMA film surface and the scratch hardness increased to 3H due to irreversible photocrosslinking of the cinnamoyl groups.

The scratch hardness of the PCEMA films under different irradiation conditions estimated the healing possibilities by controlling surface hardness. Table 4.1 summarizes the results of the scratch hardness experiments. As mentioned above, pristine PCEMA film showed a scratch hardness of 2H. After UV irradiation with 365 nm for 24 h, the PCEMA film hardened and the surface hardness increased to 4H. Various irradiation times were tested from 5 min to 24 h on the crosslinked PCEMA film to induce the photocleavage reaction only with UV irradiation of 254 nm. Among them, PCEMA film treated for 15 min showed the softest scratch hardness value of 3H. If the films were

treated longer than 120 min by 254 nm UV irradiation, the crosslinking reaction occurred simultaneously with the photocleavage reaction and induced and increase in surface hardness to 4H. The healing properties with hardness control illustrated in Figure 4.6 were evaluated, and Figure 4.7 shows the results of the overall healing process. The left part of Figure 4.7 is an OM image of damaged hard film as expressed in Figure 6 and the right part of Figure 4.7 is an OM image of healed hard film. Surface softening, healing by heat, and surface hardening resulted in healable polymethacrylate films with different surface hardness. Because both heating and UV irradiation could be applied to a small area, this approach is a very promising method for practical applications.

4.4. Conclusions

Reversible hardness-controlled polymethacrylate derivatives were synthesized and successfully applied to obtain a healable polymer film. By considering systematic studies on a series of polymethacrylate films having different T_g values, heating at modest temperature was used as a healing method, and surface hardness was controlled using cinnamoyl moeities via a reversible photocycloaddition reaction. Macroscale morphological changes during the healing process were successfully achieved with moderate temperatures. With issues related to T_g and healing properties with general polymethacrylate, this new concept of using thermoplastic polymers as healable materials opens the way for future exploration.

Table 4.1. Pencil scratch hardness of polymer films and treated PCEMA films

Sample	PEMA	PBMA	PHMA	PHEMA	PCEMA
Scratch hardness	2H	3B	< 7B	3H	2H
PCEMA with treatment	80 ^{o}C heating	365 nm UV light (24 h)	254 nm UV light (24 h)	365 nm UV light (24 h)+ 254 nm UV light(15 min)	365 nm UV light (24 h)+ 254 nm UV light (24 h)
Scratch hardness	2H	4H	3H	3H	4H

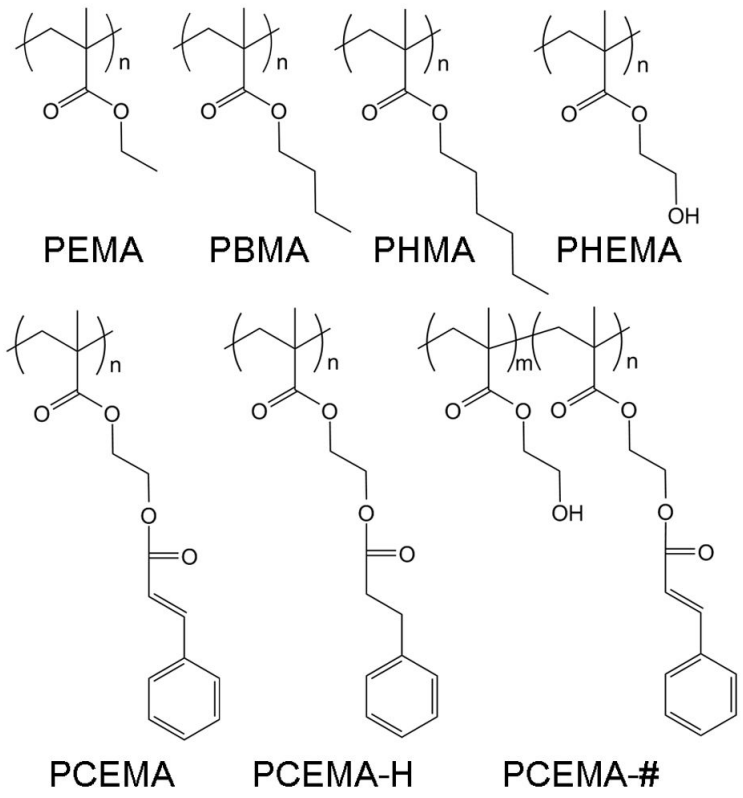

Figure.4.1. Representative chemical structure of the polymers used in this study.

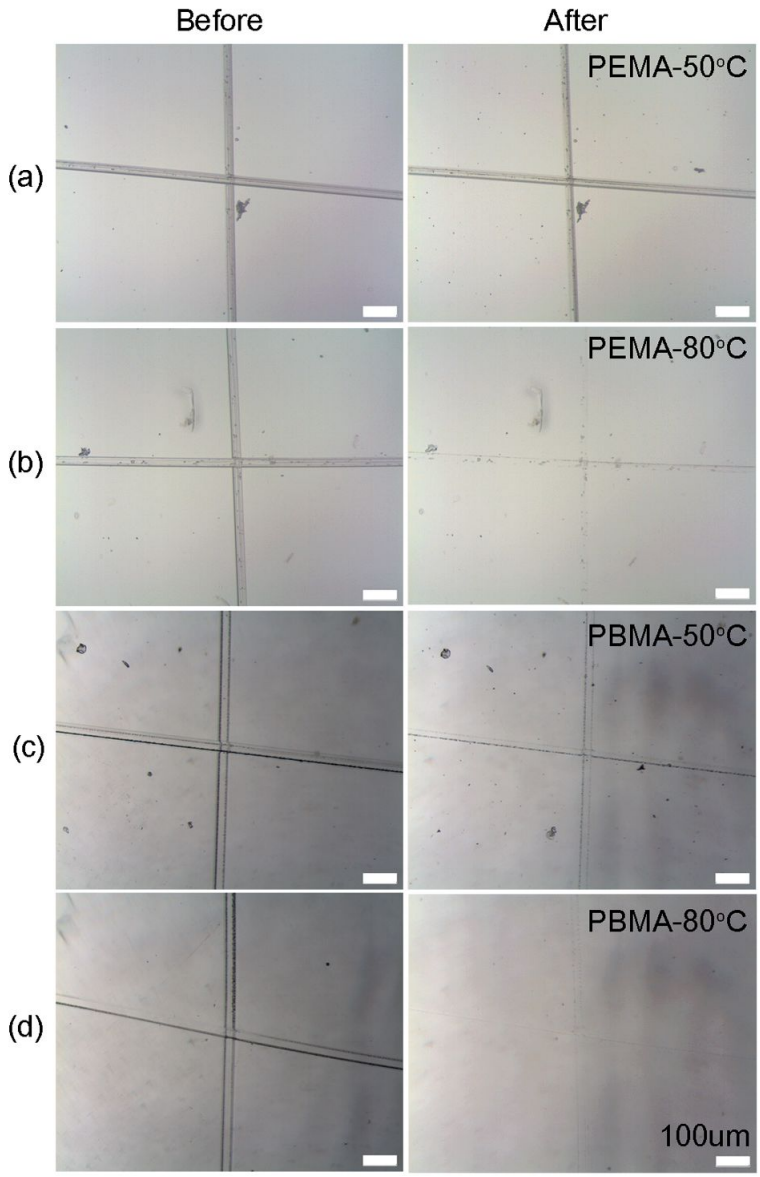

Figure.4.2. Self-healing study of PEMA and PBMA at different temperatures. Optical micrographs of the PEMA films healed at (a) 50 ^{o}C and (b) 80 ^{o}C and the PBMA films healed at (c) 50 ^{o}C and (d) 80 ^{o}C.

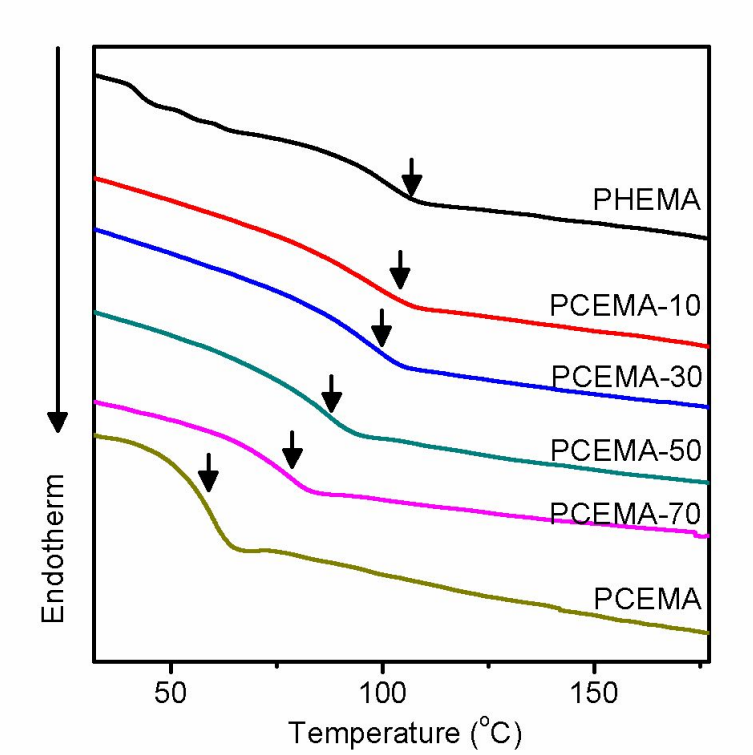

Figure.4.3. DSC curves of synthesized polymers (The black arrows indicate the glass transition temperature).

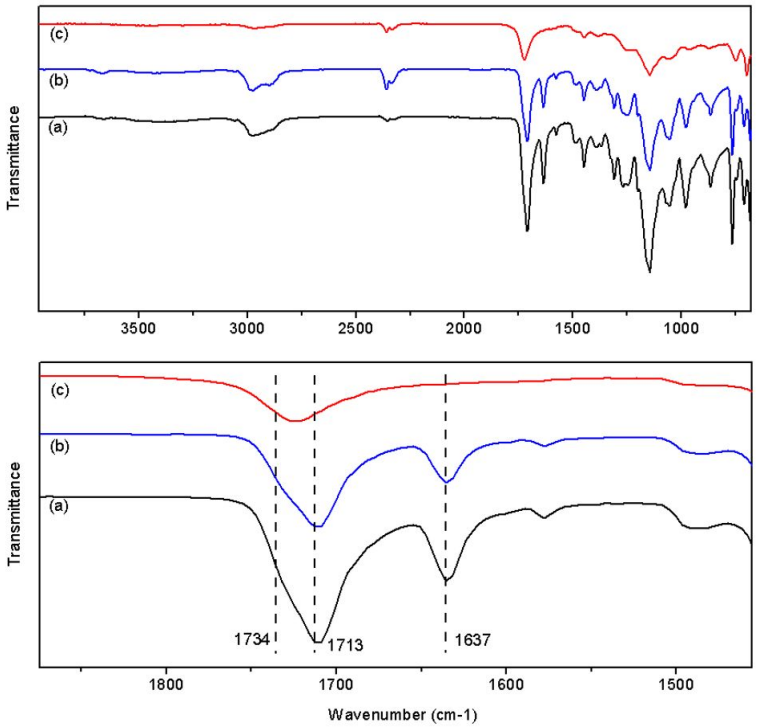

Figure.4.4 ATR-IR spectra of PCEMA: (a) pristine, (b) after heating at 80 ^{o}C for 24 h and (c) after irradiation for 24 h.

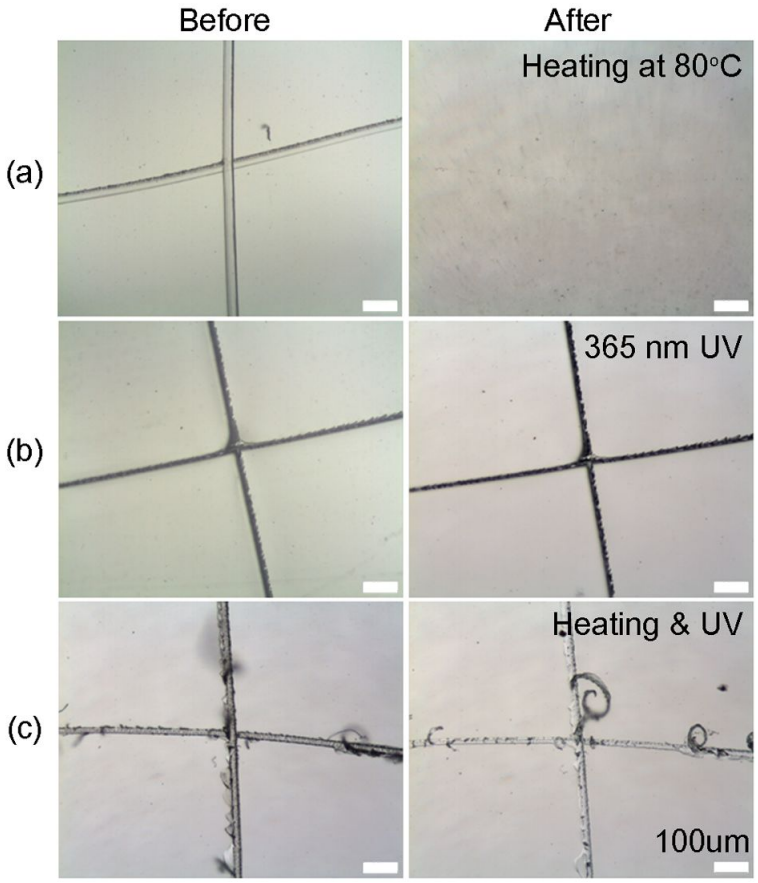

Figure.4.5. Optical micrographs of PCEMA films treated by (a) heating, (b) UV irradiation, and (c) a mixture of both.

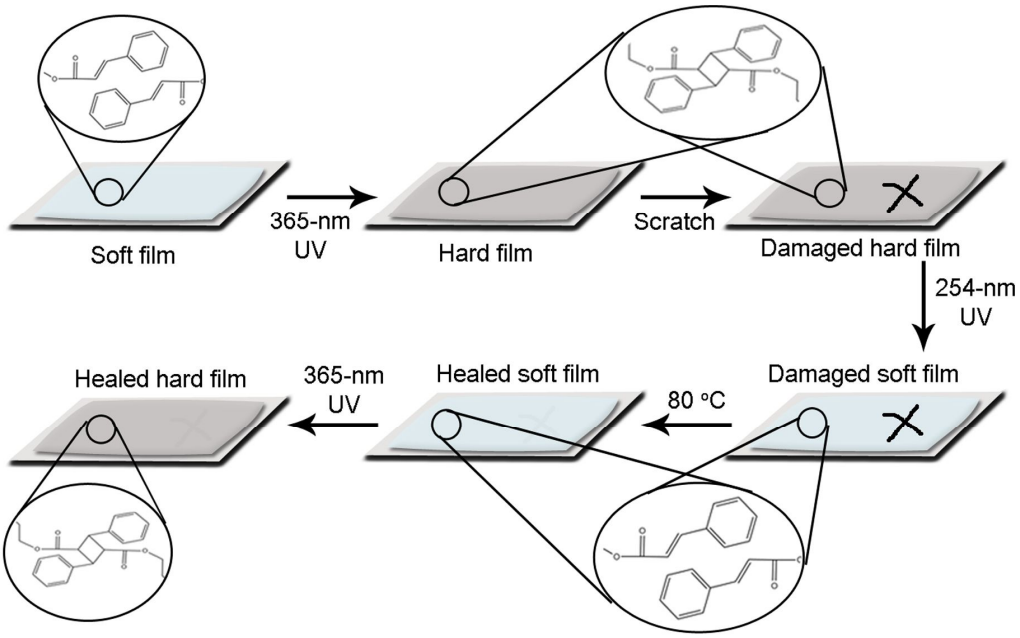

Figure.4.6. Illustration summarizing the concept of healable polymer film with controlling the surface hardness.

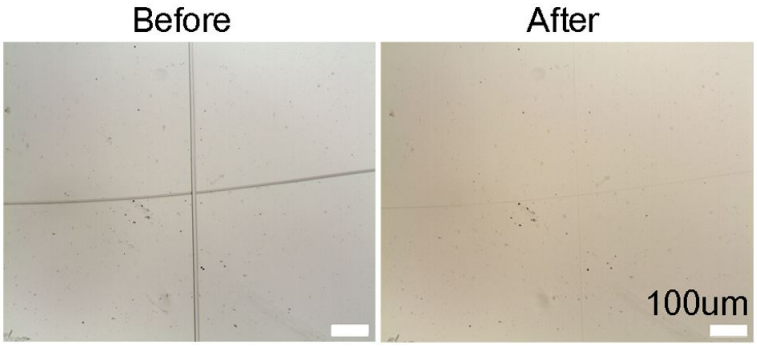

Figure.4.7. Optical micrographs of PCEMA films before (left) and after (right) overall healing process illustrated in Figure.4.6.

4.5. References

[1] Wu, D. Y.; Meure, S.; Solomon, D. *Prog. Polym. Sci.* **2008**, *33*, 479.

[2] Murphy, E. B.; Wudl, F. *Prog. Polym. Sci.* **2010**, *35*, 223

[3] Burattini, S.; Greenland, B. W.; Chappell, D.; Colquhoun, H. M.; Hayes, W. *Chem. Soc. Rev.* **2010**, *39*, 1973.

[4] Hager, M. D.; Greil, P.; Leyens, C.; Van Der Zwaag, S.; Schubert, U. S. *Adv. Mater.* **2010**, *22*, 5424.

[5] Cordier, P.; Tournilhac, F.; Soulie-Ziakovic, C.; Leibler, L. *Nature* **2008**, *451*, 977.

[6] Burnworth, M.; Tang, L.; Kumpfer, J. R.; Duncan, A. J.; Beyer, F. L.; Fiore, G. L.; Rowan, S. J.; Weder, C. *Nature* **2011**, *472*, 334.

[7] Chen, X.; Dam, M. A.; Ono, K.; Mal, A.; Shen, H.; Nutt, S. R.; Sheran, K.; Wudl, F. *Science* **2002**, *295*, 1698.

[8] Tian, Q.; Yuan, Y. C.; Rong, M. Z.; Zhang, M. Q. *J. Mater. Chem.* **2009**, *19*, 1289.

[9] Zhang, Y.; Broekhuis, A. A.; Picchioni, F. *Macromolecules* **2009**, *42*, 1906.

[10] Ghosh, B.; Urban, M. W. *Science* **2009**, *323*, 1458.

[11] Chung, C.-M.; Roh, Y.-S.; Cho, S.-Y.; Kim, J.-G. *Chem. Mater.* **2004**, *16*, 3982.

[12] White, S. R.; Sottos, N. R.; Geubelle, P. H.; Moore, J. S.; Kessler, M. R.; Sriram, S. R.; Brown, E. N.; Viswanathan, S. *Nature* **2001**, *409*, 794.

[13] Cho, S. H.; Andersson, H. M.; White, S. R.; Sottos, N. R.; Braun, P. V. *Adv. Mater.* **2006**, *18*, 997.

[14] Toohey, K. S.; Sottos, N. R.; Lewis, J. A.; Moor, J. S.; White, S. R. *Nat. Mater.* **2007**, *6*, 581.

[15] Wang, H. P.;Yuan, Y. C.; Rong, M. Z.; Zhang, M. Q. *Macromolecules* **2010**, *43*, 595.

[16] Canadell, J.; Goossens, H.; Klumperman, B. *Macromolecules* **2011**, *44*, 2536.

[17] Rodriguez, E. D.; Luo, X.; Mather, P. T. *ACS Appl. Mater. Interfaces* **2011**, *3*, 152.

[18] Froimowicz, P.; Frey, H.; Landfester, K. *Macromol. Rapid Commun.* **2011**, *32*, 468.

[19] Kavitha, A. A.; Singha, N. K. *ACS Appl. Mater. Interfaces* **2009**, *1*, 1427.

[20] Peterson, A. M.; Jensen, R. E.; Palmese, G. R. *ACS Appl. Mater. Interfaces* **2010**, *2*, 1141.

[21] Kim, Y. H.; Wool, R. P. *Macromolecules* **1983**, *16*, 1115.

[22] Mcgarel, O. J.; Wool, R. P. *J. Polym. Sci. Polym. Phys.* **1987**, *25*, 2541.

[23] Willett, J. L.; Wool, R. P. *Macromolecules* **1993**, *26*, 5336.

[24] Boiko, Y. M.; Purdhomme, R. E. *Macromolecules* **1997**, *30*, 3708.

[25] Boiko, Y. M.; Guerin, G. Marikhin, V. A.; Purdhomme, R. E. *Polymer* **2001**, *42*, 8695.

[26] Boiko, Y. M. *Colloid Polym. Sci.* **2011**, *289*, 1847.

[27] Guevin, P. R.; Coat. Jr., J. *Technol.* **1995**, *67*, 61.

[28] Chen, Z.; Wu, L. Y. L.; Chwa, E.; Tham, O. *Mat. Sci. Eng. A* **2008**, *493*, 292.

[29] Kilburn, D.; Dlubek, G.; Piontech, J.; Alam, M. A. *Polymer* **2006**, *47*, 7774.

[30] De Gennes, P.-G. *J. Chem. Phys.* **1971**, *55*, 572.

[31] Lee, J.-C.; Litt, M. H.; Rogers, C. E. *Macromolecules* **1998**, *31*, 2440.

[32] Chung, J.-S.; Kim, B. G.; Sohn, E.-H.; Lee, J.-C. *Macromolecules* **2010**, *43*, 10481.

[33] Sohn, E.-H.; Kim, S. H.; Lee, M.; Lee, J.-C.; Song, K. *J. Colloid Interface Sci.* **2011**, *360*, 623.

[34] Van Krevelen, D. W. Properties of Polymers, third ed., Elsevier Science, New York, 1990. Pp. 129-188.

[35] Sung, S.-J.; Cho, K.-Y.; Hah, H.; Lee, J.; Shin, H.-K.; Park, J.-K. *Polymer* **2006**, *47*, 2314.

[36] Cho, S.-Y.; Kim, J.-G.; Oh, S.-Y.; Chung, C.-M. *Macromolecular Research* **2010**, *18*, 212.

[37] Ikeda, R.; Tanaka, H.; Uyama, H.; Kobayashi, S. *Polymer Journal*, **2000**, *32*, 589.

[38] Andreopoulos, F. M.; Beckman, E. J.; Russell, A. J. *J. Polym. Sci. Part A Polym. Chem.* **2000**, *38*, 1466.

[39] Chen, Y.; Chen, K.-H. *J. Polym. Sci. Part A Polym. Chem.* **1994**, *32*, 1867.

Chapter 5

Thermo-Responsive Copolymers with Ionic Group as Novel Draw Solutes for Forward Osmosis Processes

5.1. Introduction

Forward osmosis (FO) process which driven by osmotic pressure has been intensively studied for its use in desalination, water reuse and power generation.[1-3] FO utilizes the osmotic pressure difference of two solutions separated by a semi-permeable membrane to induce spontaneous movement of water molecules from the less concentrated solution to the other solution. Comparing with reverse osmosis (RO) process which also have become a growing area of water purification field, FO process only requires the net energy in the separation and recycling of draw solutes so that the energy efficiency of FO process is far better than RO process. Natually driven osmotic flow can be used at a low cost due to the absence of artificial pressures and additionally, low membrane fouling with high rejection properties can be obtained for FO process.[4-6]

Semi-permeable membranes with high water flux and rejection play an important role in FO process and lots of efforts have been devoted to prepare the eligible membranes. Likewise, the selection of a suitable draw solute can greatly influence the efficiency of FO process.[7-10] In general, entitled draw solutes possess the qualities of being able to generate high osmotic pressures and easy separation from resulting water. A number of draw solutes such as NaCl, $MgCl_2$, and ammonium carbonate have been studied to develop the appropriate draw solutions due to their good water solubility and high osmotic pressure. However, these small salts and ammonium carbonate show high reverse solute diffusion across the semi-permeable membrane, and require high energy cost for recycle. Sugars also used for draw solute because these materials show very low reverse

solute diffusion but they show lower osmotic pressures than other salts. Recently, new magnetic nanoparticles and hydrogels were developed for FO draw solute to overcome the weak points of the previous solutes.[11-14]

Among the various efforts to find the suitable draw solute, we decide to use a thermo-responsive copolymer with ionic group in order to fulfill the required characteristics of suitable draw solutes. Recently, J.-F. Lutz and collegues present the candidate polymers expecting to replace the poly(*N*-isopropylacrylamide) (PNIPAM) which is a most famous and widely used polymer in a lower critical solution temperature (LCST) fields.[15-17] They reported that methacrylate polymers with ethylene glycol side group show clear LCST behavior. Furthermore these polymers show very good reversibility and have narrow transition gap compared with NIPAM.

With this novel LCST polymer, we planed to conduct the copolymerization with ionic polymer. There have been few reports on the correlation between ionic polymer and osmotic pressure, and especially a few reports of systematic studies on the relationship among polymer structures, osmotic pressure and draw solute properties has been located.[18] The target of the present article is to illustrate that copolymers of LCST group and ionic group could be a novel draw solute for FO process. This study systematically synthesized a series of ionic polymers and copolymers having LCST. The osmotic pressures of polymer draw solutes in water were investigated. Furthermore, synthesized polymers having relatively high osmotic pressures were tested in FO process as a draw solute.

5.2. Experimental

Materials

Two kinds of monomers, [2-(methacryloyloxy)ethyl] trimethylammonium chloride (MTAC, 80 wt% in H_2O) and 2-(2-methoxyethoxy)ethyl methacrylate (MEO_2MA, 95 %), were purchased from Sigma-Aldrich Chemical Co. The purchased monomers were purified by filteration of alumina column chromatography with a membrane filter. MTAC aqueous solution was precipitated in acetone to remove a water. Copper chloride, 2,2'-bypyridyl, methyl 2-bromopropionate and 2,2-azobis(2-methylpropionamidine) dihydrochloride (Vazo-56) were also perchased from Sigma-Aldrich Chemical Co. Azobisisobutyronitrile (AIBN) was purchased from TCI. All reagents and solvents were used without further purification.

Synthesis

Preparation of homopolymers using atom transfer radical polymerization (ATRP)

Homopolymers were prepared by ATRP based on a method described in the literature.[19-20] A 100 mL dried Schlenk flask containing a magnetic stirrer bar was charged with CuCl (9.9 mg, 0.1 mmol), methyl 2-bromopropionate (16.6 mg, 0.1 mmol), monomers (10 mmol) and solvent (5 mL). Ethanol was used as a solvent for homopolymerization of MEO_2MA and water/isopropyl alcohol mixture was used for that of MTAC. The mixture was degassed three times using the freeze-pump-thaw cycle. After complete degassing, a ethanol or isopropyl alcohol solution (1 mL) of 2,2'-bipyridyl

(15.6 mg, 0.2 mmol) was injected into the mixture to initiate the reaction. The mixture was at 60 ^{o}C and then poured into hexane to precipitate the product. The polymerization time was varied to control the molecular weights. The reaction solution turned blue on exposure to air, indicating aerial oxidation of the Cu(I) catalyst. The resulting polymer was diluted with water/ethanol and then passed through an alumina column to remove the spent ATRP catalyst. The polymer solution was dried under vacuum to remove the solvent. This product was obtained in > 50 % yield after the purification steps.

Preparation of copolymer series

A series of P(MEO_2MA-r-MTAC) copolymers was synthesized from identical procedure described above except the amount of monomers to control the copolymer composition. The concentration of MEO_2MA (9.5 – 7 mmol) and MTAC (0.5 – 3 mmol) were varied, but their sum was fixed to be 10 mmol. We calculated the monomer composition in the synthesized polymers using the ^{1}H NMR results by comparing the multiplet at 4.05 (2H) from the methyl ether of MEO_2MA and the multiplet at 4.37 (2H) from that of MTAC.

Preparation of homopolymers using free radical polymerization

Homopolymers were also prepared by conventional free radical polymerization in ethanol or water using AIBN or VAZO-65 as an initiator.[21] Calculated amount of monomers of MEO_2MA and MTAC and initiator (typically 1wt % with monomer) were

placed in round bottle with solvents. The solution was bubbled with nitrogen for several minutes and heated at 60 ^{o}C while being slowly rotated to provide mixing. The polymer was isolated and purified by precipitation in methanol or acetone. The purified polymer was then dried in a vacuum oven at room temperature. Copolymers of MEO_2MA with MTAC were also prepared in this fashion.

Analysis

The ^{1}H NMR spectra (500 MHz) were measured in D_2O using Bruker, Avance 500. The molecular weights (M_n) and polydispersity index were obtained on a Waters gel permeation chromatography instrument (GPC) equipped with TSKgel G5000PWxl-cP, TSKgel G3000PWxl-CP columns and a Waters 410 differential refractometer detector. 0.1 M $NaNO_3$ aquous solution was used as a eluent at a flow rate 1 mL/min at 35 ^{o}C. A calibration plot was constructed using poly(ethylene glycol) and poly(ethylene oxide) standards (molecular weights ranged from 1,500 to 520,000). The osmotic pressure was measured by a freezing-point depression method with an semi-micro osmometer K-7400 (KNAUER, Germany). The LCST phase transitions of solutions containing thermo-sensitive polymers were measured by a UV-Vis spectrophotometer at a concentration of 3 mg/ml as the temperature was increased stepwise at a rate of 1 ^{o}C min^{-1}. By increasing the temperature, the transmittance at a wavelength of 650 nm was measured to determine the phase transition temperature. The phase transition temperature was defined at which the transmittance was below 5%.

5.3. Results and Discussions.

Figure 5.1 shows the schematic diagram proposed for explaining the thermo-responsiveness of P(MEO_2MA-r-MTAC) copolymers with ionic moieties. In order to fulfil the required characteristics of draw solutes in FO, copolymer must possess both highly ionized groups to induce osmotic pressures and extremely thermo-responsive polymers to facilitate easy recycle via simple heating. For most of the polymers exhibiting an aqueous LCST, the thermo-responsive behavior generally results from a subtle balance between favorable and unfavorable interactions in water.[15-17] If the FO system works at temperatures less than the LCST, thermo-responsive polymer can be used as a draw solute with good solubility and also it is easy to separate for recycle at higher temperatures. Increasing the temperature to above the LCST reduces the polymer solubility in water then filtration or precipitation should be possible. Furthermore, the introduction of ionic part in the copolymer should increase the solubility in water and generate the high osmotic pressure.

Homo and copolymers were both prepared via atom transfer radical polymerization (ATRP). Initiators and catalysts were carefully selected in order to obtain the polymers with a comparable degree of polymerization and compositions. The synthesis of a series of water-soluble polymer were determined by a combination of techniques, including ^{1}H nuclear magnetic resonance spectroscopy (NMR), gel permeation chromatography (GPC), and comparisons of the solution properties of the polymers with UV-Vis

spectrophotometer and semi-micro osmometer.

To evaluate the synthesized polymers as draw solutes, we measured osmotic pressure using osmometer. NaCl is a widely used draw solute in FO system and tested as a reference. In general, the osmotic pressure is a colligative properties, which means that it is proportional to the concentration of solute. So the important point of the figure including effect of concentration on the osmotic pressure is a slope. For example, if the salts such as NaCl and MTAC in the solution ionized perfectly to 2 molecules, 2 molar amount of molecules exist in the 1mol concentration solution then reveals with a slope value, 2. As can be seen in Figure 5.2, NaCl and MTAC, reference salt and monomer of PMTAC, respectively, are fully ionized and show the high osmotic pressure, near the 2 osmol/kg at 1 mol/L.

Before the copolymerization, the homopolymerizaion of PMTAC was conducted to optimize the polymerization condition for draw solutes. With identical synthetic procedure, polymerization time was varied from 10 min to 24 h to control the molecular weight of polymers. The monomer of PMTAC, MTAC shows even higher osmotic pressure than NaCl at same concentration which indicates that this monomer is a suitable candidate for draw solute. After the polymerization, it is observed that the values of the osmotic pressure were decreased with increasing the polymerization time. The osmotic pressure of PMTAC at 1 mol/L was decreased for 7.5 % and 17.1 % after 30 min and 60 min, respectively. After the 24 h polymerization, the osmotic pressure was reduced to 57.8 % compared with monomer MTAC. The osmotic pressure was decreased with

increasing the polymerization time indicating that the short polymerization times are required to produce high osmotic pressure because the molecular weight is inversely proportional to osmotic pressure.[22-23] The increase of molecular weight should increase the relative viscosity and decrease the degree of ionization in water solution which also affect on the osmotic pressure. This may imply that the polymer draw solute with a small molecular weight will have better performance if being used as the draw solute. Based on the osmotic pressure values of PMTAC with different polymerization time, we determined the 60 min for optimal polymerzation time which have suitable osmotic pressure and polymeric properties. If we use too low molecular weight polymer for draw solute, we might be missing the advantages of using polymers such as ease of separation and low reverse diffusivity. Additionally, there should be exist the minimum molecular weight to obtain the LCST behavior.

Another part of the copolymer, $PMEO_2MA$, which has LCST was also prepared via ATRP with identical procedure of PMTAC except solvent, ethanol instead of water/isopropyl alcohol mixture. The synthesis and solution properties of this interesting polymer and copolymers with oligo(ethylene glycol) methacrylate are already reported .[15-17] They present that the LCST of these polymers could be accurately tuned by adjusting the initial composition of the comonomer feed and exhibit a excellent solution properties generally comparable, and in some cases, superior to PNIPAM, which has been the most studied thermosensitive polymer in various applications. For homopolymer $PMEO_2MA$, LCST of 25 ^{o}C was measured despite of the short

polymerization time, which are in good agreement with previously reported values and exhibits a uniform thermal transition profile (narrow hysteresis between heating and cooling). If the solution temperature increased to above LCST, the solubility of $PMEO_2MA$ was decreased and separation process using PTFE syringe filter (pore size: 0.45 um) was available.

By taking into account the results of homopolymerization, synthesis and characterization of the copolymer P(MEO_2MA-r-MTAC) were studied. In this study, we synthesized the copolymers with the composition of MEO_2MA:MTAC from 70:30 to 95:5. Identical synthetic procedures were used with PMTAC homopolymer and polymerization time was fixed to 60 min. Table 1 shows the composition and the properties of a series of P(MEO_2MA-r-MTAC) copolymers.

Table 5.1 and Figure 5.3 report the values of LCST measured for aqueous solutions of either the $PMEO_2MA$ and a series of copolymers. For homopolymer $PMEO_2MA$, LCST point of 25 ^oC was measured, which are in good agreement with previously reported values.[15] For a series of copolymers, as expected easily, the LCST values dramatically increased as the MTAC portions increased. Measured LCST values were comprised in the range 25 - 65 ^oC. Visually, it was easy to observe the sharp transition between a transparent and cloudy solution with increasing temperature. Because the PMTAC does not show the LCST, LCST values increase with the molar fraction of MTAC in the copolymer and not observed when the portion of MTAC reaches to 30 mol %. Because the LCST behavior is very sensitive on the polymer structure and it is sure that the

increase of MTAC portion should ruin the LCST behavior. For the ease of separation, a proper low content of MTAC should be controled to obtain the suitable LCST point. On the contrary, high content of MTAC should be required because the MEO_2MA part does not help the osmotic properties. Figure 5.4 shows the osmotic pressure of homo- and copolymers with different monomer composition. The $PMEO_2MA$ homopolymer shows very low osmotic pressure compared with PMTAC for all measured concentration despite of the small molecular weight. With increasing the content of MTAC part, the osmotic pressure increases dramatically and the CO80 and CO75 shows the proper osmotic pressure values in the middle between PMTAC and $PMEO_2MA$ homopolymer despite of the relatively small content of MTAC. We speculated that the osmotic pressure of CO80 and CO75 would be considerable to use as a novel polymer draw solute and this polymer also shows the proper LCST for separation process.

5.4. Conclusions

We have demonstrated novel polymer draw solutes of using thermo-responsive copolymer in the FO process. Experimental results imply that the PMTAC homopolymer shows extremly high osmotic pressure and $PMEO_2MA$ homopolymer shows the possibility of recycling. After the copolymerization, their designed structures provide relative high osmotic pressures and ease in recycle via an ultrafilteration process with moderate heating condition. Thus, P(MEO_2MA-r-MTAC) copolymers can be considered as ideal structures, which conbine both the properties of ionic group and LCST group in a single macromolecules. Hence, these novel thermal-responsive copolymers are very relevant for many applications in material science and biotechnology.

Table 5.1. Properties of copolymers of MEO_2MA and MTAC

Sample	MEO_2MA/MTAC		Molecular weight (M_n)	PDI (M_w/M_n)	LCST (^oC)
	Feed (mol%)	In polymer (mol%) [a]			
CO95	95/5	94/6	2,300	2.29	32
CO90	90/10	85/15	2,800	2.20	39
CO85	85/15	82/18	3,200	2.35	47
CO80	80/20	75/25	3,000	2.41	51
CO75	75/25	70/30	11,200	1.37	65
CO70	70/30	62/38	10,600	1.53	[b]

[a] Overall monomer conversion measured by ^1H NMR.

[b] LCST was not observed up to 80 ^oC.

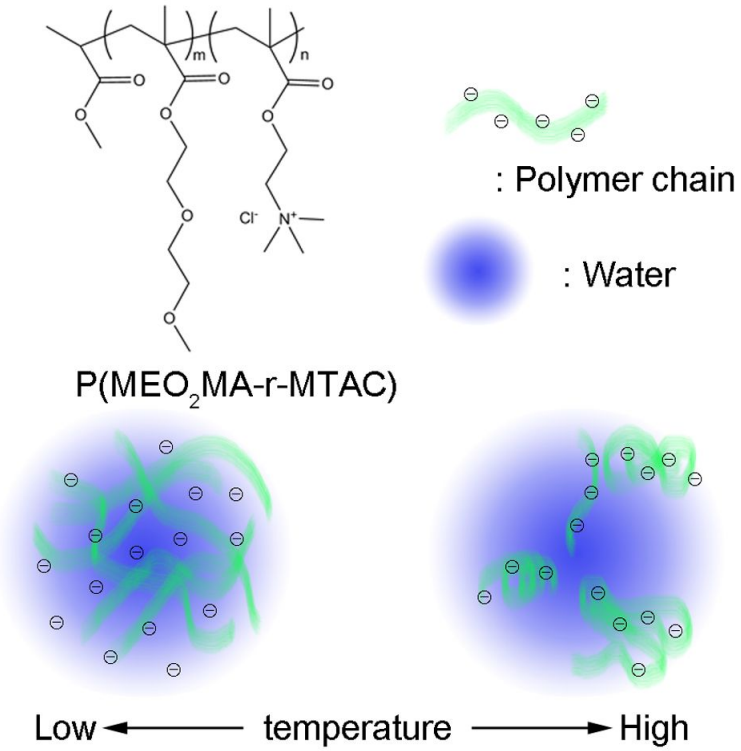

Figure 5.1. Schematic representation of the P(MEO_2MA-r-MTAC) copolymer in water with different temperatures.

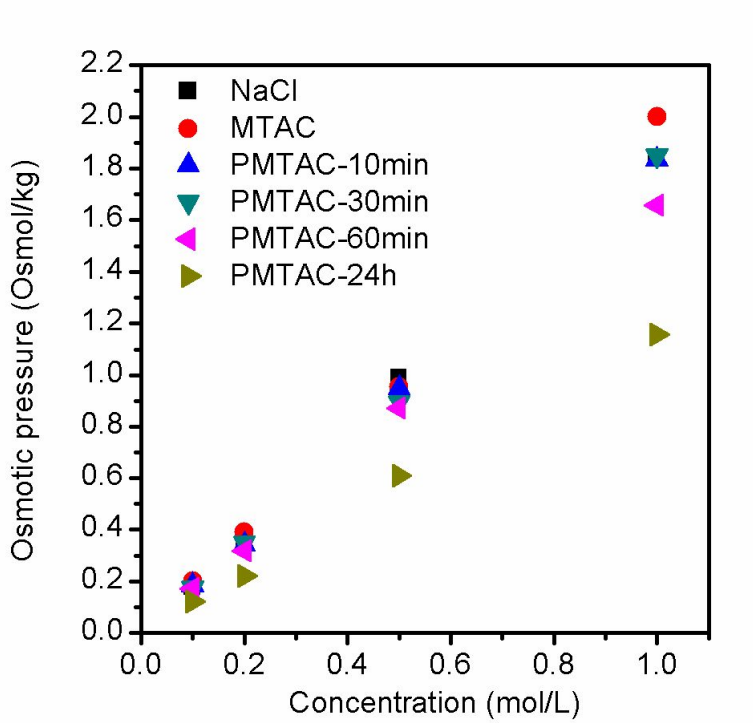

Figure. 5.2. Osmotic pressure of NaCl, MTAC and PMTAC homopolymer with different polymerization time. Plots of transmittance as a function of temperature (650 nm) measured for aqueous solutions (3 mg/mL) of $PMEO_2MA$ and a series of copolymers.

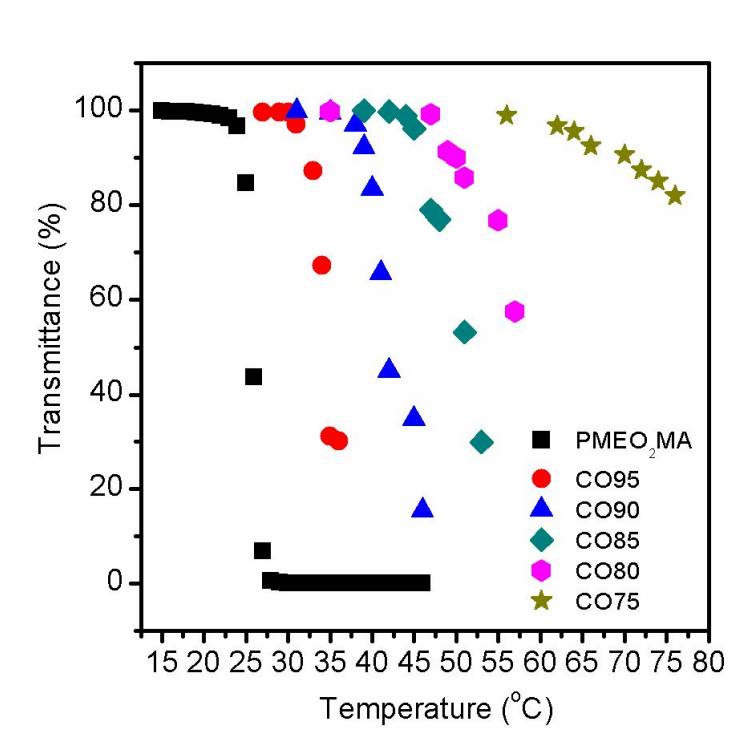

Figure. 5.3. Plots of transmittance as a function of temperature (650 nm) measured for aqueous solutions (3 mg/mL) of $PMEO_2MA$ and a series of copolymers.

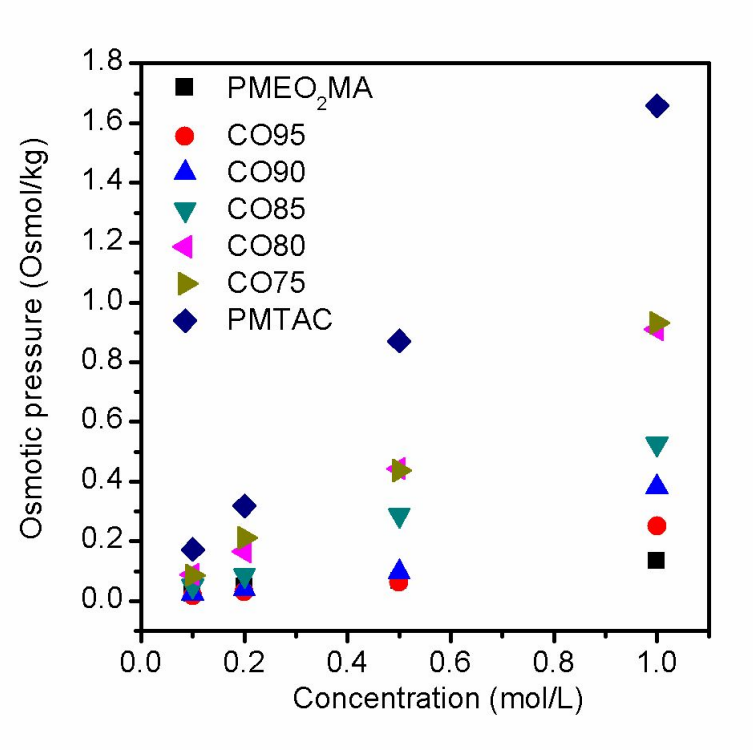

Figure. 5.4. Osmotic pressure of PMEO2MA, P(MEO2MA-r-MTAC)s and PMTAC. (polymerization time: 60 min)

5.5. References

[1] Mcginnis, R. L.; Elimelech, M. *Environ. Sci. Technol*. **2008**, *42*, 8625.

[2] Hoover, L. A.; Phillip, W. A.; Tiraferri, A.; Yip, N. Y.; Elimelech, M. *Environ. Sci. Technol*. **2011**, *45*, 9824.

[3] Gerstandt, K.; Peinemann, K. V.; Skilhagen, S. E.; Thorsen, T.; Holt, T. *Desalination*, **2008**, *224*, 64.

[4] Su, J. C.; Yang, Q.; Teo, J. F.; Chung, T.-S. *J. Membr. Sci.* **2007**, *300*, 6.

[5] Li, D.; Wang, H. T. *J. Mater. Chem.* **2010**, *20*, 4551.

[6] Cath, T. Y.; Childress, A. E.; Elimelech, M. *J. Membr. Sci.* **2006**, *281*, 70.

[7] Kessler, J. O.; Moody, C. D. *Desalination*, **1975**, *18*, 297.

[8] Kravath, R. E.; Davis, J. A. *Desalination*, **1975**, *16*, 151.

[9] McCutcheon, J. R.; McGinnis, R. L.; Elimelech, M. *Desalination*, **2005**, *174*, 1.

[10] McCutcheon, J. R.; McGinnis, R. L.; Elimelech, M. *J. Membr. Sci.* **2006**, *278*, 114.

[11] Ling, M. M.; Wang, K. Y.; Chung, T.-S. *Ind. Eng. Chem. Res*. **2010**, *49*, 5869.

[12] Ling, M. M.; Chung, T.-S.; Lu, X. *Chem. Commun.* **2011**, *47*, 10788.

[13] Li, D.; Zhang, X.; Yao, J.; Simon, G. P.; Wang, H. *Chem. Commun.* **2011**, *47*, 1710.

[14] Li, D.; Zhang, X.; Yao, J.; Simon, G. P.; Wang, H. *Soft Matter* **2011**, *7*, 10048.

[15] Lutz, J.-F.; Akdemir, O.; Hoth, A. *J. Am. Chem. Soc.* **2006**, *128*, 13046.

[16] Lutz, J.-F.; Hoth, A. *Macromolecules* **2006**, *39*, 893.

[17] Lutz, J.-F. *Adv. Mater.* **2011**, *23*, 2237.

[18] Ge, Q.; Su, J.; Amy, G. L.; Chung, T.-S. *Water Research* **2012**, *46*, 1318.

[19] Li, Y.; Armes, S. P.; Jin, X.; Zhu, S. *Macromolecules* **2003**, *36*, 8268.

[20] Kobayashi, M.; Terada, M.; Terayama, Y.; Kikuchi, M.; Takahara, A. *Macromolecules* **2010**, *43*,8409.

[21] Burke, N. A. D.; Mazumder, M. A. J.; Hanna, M.; Stover, H. D. H. *J. Polym. Sci. Part A: Polym. Chem.* **2007**, *45*, 4129.

[22] Fort, R. J.; Polyzoidis, T. M. *Europ. Polym. J.* **1976**, *12*, 685.

[23] Money, N. P. *Plant Physiol.* **1989**, *91*, 766.

초 록

본 연구에서는 플루오로 알킬기를 측쇄로 가지는 빗살형 고분자와 시나모일기 또는 올리고(에틸렌 글라이콜)기를 측쇄로 가지는 자극 응답성 고분자를 합성하고 분석하였으며 낮은 표면 에너지 고분자, 자가 복원성 고분자, 고분자 유도 용액 등과 같은 응용 분야로의 적용 가능성에 대해서 모색하였다. 빗살형 불소 고분자는 고유의 낮은 표면에너지 때문에 전자재료, 접착 방지 코팅, 그리고 의약 재료 등과 같은 다양한 분야에서 응용 되고 있으며 다양한 방법으로 불소 고분자를 합성하려는 노력이 이루어지고 있다. 또한 자극 응답성 고분자는 주변의 화학적, 물리적 자극에 반응하여 고분자 구조나 성질을 변화시키는 특성을 가지고 구조 변화, 이온 혹은 분자 전달, 젖음성 변화, 그리고 접촉 성질 변화 등과 같은 다양한 현상을 보이게 된다. 이러한 고분자는 약물 전달이나 진단, 조직 공학, 자가 복원성 고분자와 같은 시스템에서 적용을 시도 되고 있다.

먼저 본 연구에서는 측쇄에 플루오로 알킬기를 가지는 폴리옥시에틸렌계 고분자를 합성하여 플루오로 알킬기의 함유량에 따른 표면 구조 변화를 확인하였다. 또한 이러한 표면 구조의 변화가 표면 에너지에 미치는 영향을 살펴보고 그 상관 관계를 도출하고자 하였다. 다양한 플루오로 알킬기 함유량을 가지는 고분자 중 플루오로 알킬기가 58 % 이상 함유 된 빗살형 고분자들이 열에 의해 어닐링 되었을 때 매우 낮은 표면 에너지를 가지는 것이 확인 되었으며 이때 고분자 표면에서의 파라크리스탈 구조의 배열이

매우 좋아지는 것을 확인할 수 있었다.

두번째, 초소수성과 방오, 항균 성질을 가지는 은-플루오로 알킬 복합체에 대해서 연구하였다. 은 염과 퍼플루오로티올의 간단한 반응을 통해 형성된 이 복합체는 그 반응 비율이 1:2 이상일 때 계층적인 마이크로/나노 사이즈의 와이어 형태로 구조가 만들어 졌으며, 이러한 복합체는 초소수성과 함께 박테리아에 대한 방오 성질을 가지는 것을 확인하였다. 또한 UV 조사를 통해 와이어 구조 표면위에 은 나노 입자를 형성 시킬 수 있었으며 항균 성질 또한 구현해 낼 수 있었다.

세번째, 빛에 반응하여 표면 강도가 달라지는 메타아크릴레이트계 고분자 필름을 형성하여 복원성을 가지는 필름으로의 응용 가능성에 대한 연구를 진행하였다. 빛에 응답하는 시나모일기를 측쇄에 가지고 가역적인 가교 반응을 통해 표면 강도를 조절 할 수 있게 디자인 된 고분자는 유리전이온도를 조절함으로써 적당한 온도에서 상처가 나도 복원이 가능하도록 하였다. UV 조사를 통해 상처난 필름의 강도를 낮추고, 적절한 열을 가해 상처를 복원, 마무리로 다시 UV를 조사하여 가교 시킴으로서 고유의 강도로 복원하는 시스템을 고안하여 성공적으로 복원이 가능한 필름을 구현할 수 있었다.

마지막으로 측쇄에 올리고(에틸렌 글라이콜)기를 포함하여 LCST 성질을 보이는 고분자를 합성하고 이온성기를 측쇄로 가지는 고분자와 공중합을 통해 정삼투 시스템의 유도 용액으로 사용 가능한 고분자를 합성하였다. 열에 반응하는 고분자와 이온성을 가지고 높은 삼투압을 유발할 수 있는 고분자의

공중합을 통해 적절한 삼투압과 LCST 수치를 가지는 고분자가 성공적으로 합성되었으며 그 중 올리고(에틸렌 글라이콜)기와 이온성기의 비율이 8:2 를 가지는 고분자가 정삼투압 유도 용질 분야에서 새로운 고분자 유도 용질로 사용되기에 적합할 것으로 판단 되었다.

주요어: 빗살형 불소 고분자, 은-불소 복합체, 방오 성질, 자극응답성 고분자.

학번: 2009-30250